Lawrence Berkeley National Laboratory

Title

Incorporating leaf chlorophyll content into a two-leaf terrestrial biosphere model for estimating carbon and water fluxes at a forest site

Permalink

https://escholarship.org/uc/item/2f51n0s9

Authors

Luo, Xiangzhong

Croft, Holly

Chen, Jing M

et al.

Publication Date

DOI

Peer reviewed

Incorporating leaf chlorophyll content into a two-leaf terrestrial biosphere model for estimating carbon and water fluxes at a forest site

Xiangzhong Luo [a*], Holly Croft [a], Jing M. Chen [a], Paul Bartlett [b], Ralf Staebler [c], Norma Froelich [d]

[a] Department of Geography and Planning, University of Toronto, Toronto, ON, M5S 3G3, Canada

[b] Climate Research Division, Environment and Climate Change Canada, Toronto, ON, M3H 5T4, Canada

[c] Air Quality Processes Research Section, Environment and Climate Change Canada, Toronto, ON, M3H 5T4, Canada

[d] Earth, Environmental and Geographical Sciences, Northern Michigan University, Marquette, MI 49855, USA

*Corresponding author

Xiangzhong Luo, email: xiangzhong.luo@mail.utoronto.ca

Abstract

Chlorophyll is the main light-harvesting pigment in leaves, facilitating photosynthesis and indicating the supply of nitrogen for photosynthetic enzymes. In this study, we explore the feasibility of integrating leaf chlorophyll content (Chl_{leaf}) into a Terrestrial Biosphere Model

23   (TBM), as a proxy for the leaf maximum carboxylation rate at 25°C (V_{max}^{25}), for the purpose of

24   improving carbon and water flux estimation. Measurements of Chl$_{leaf}$ and V_{max}^{25} were made in

25   a deciduous forest stand at the Borden Forest Research Station in southern Ontario, Canada,

26   where carbon and water fluxes were measured by the eddy covariance method. The use of

27   Chl$_{leaf}$-based V_{max}^{25} in the TBM significantly reduces the bias of estimated gross primary

28   productivity (GPP) and evapotranspiration (ET) and improves the temporal correlations

29   between the simulated and the measured fluxes, relative to the commonly employed cases of

30   using specified constant V_{max}^{25}, leaf area index (LAI)-based V_{max}^{25} or specific leaf area (SLA)-

31   based V_{max}^{25}. The biggest improvements are found in spring and fall, when the mean absolute

32   errors (MAEs) between modelled and measured GPP are reduced from between 2.2-3.2 to 1.8

33   g C m$_{-2}$ d$_{-1}$ in spring and from between 2.1-2.8 to 1.8 g C m$_{-2}$ d$_{-1}$ in fall. The MAEs in ET

34   estimates are reduced from 0.7-0.8 mm d$_{-1}$ to 0.6 mm d$_{-1}$ in spring, but no significant

35   improvement is noted in autumn. A two-leaf upscaling scheme is used to account for the uneven

36   distribution of incoming solar radiation inside canopies and the associated physiological

37   differences between leaves. We found that modelled V_{max}^{25} in sunlit leaves is 34% larger than

38   in the shaded leaves of the same Chl$_{leaf}$, which echoes previous physiological studies on light

39   acclimation of plants. This study represents the first case of the incorporation of chlorophyll as

40   a proxy for V_{max}^{25} in a two-leaf TBM at a forest stand and demonstrates the efficacy of using

41   chlorophyll to constrain V_{max}^{25} and reduce the uncertainties in GPP and ET simulations.

42   **Keywords**: chlorophyll; photosynthesis; terrestrial biosphere model; evapotranspiration; two-

43   leaf scheme

44

1. Introduction

Predicting gross primary productivity (GPP) and evapotranspiration (ET) has posed a challenge

for accurately quantifying the global terrestrial carbon, water and energy budgets in the context

of climate change (Jung et al., 2010; Schaefer et al., 2012). State-of-the-art terrestrial biosphere

models (TBMs) have been developed to quantify carbon and water fluxes by describing

physical and physiological processes in the soil-vegetation-atmosphere continuum. Model

validation and inter-model comparisons have suggested that TBMs are particularly sensitive to

the parameterization of leaf photosynthetic capacity (Kattge et al., 2009). Since leaf

photosynthetic parameters can only be measured directly at the leaf level (Wilson et al., 2000;

Xu and Baldocchi, 2003), using labour-intensive instruments, their limited availability in both

space and time has hindered progress in improving GPP and ET estimates by TBMs.

Consequently, finding a reliable and easily measurable proxy for leaf photosynthetic

parameters across large spatial scales is paramount for the modelling community.

Most TBMs simulate photosynthesis using an enzyme-kinetic model developed by Farquhar

(Farquhar et al., 1980). Two key parameters are used to represent the leaf photosynthetic

capacity: the maximum carboxylation capacity (V_{max}^{25}) and the maximum electron transport

capacity (J_{max}^{25}) at 25°C. V_{max}^{25} refers to the kinetic properties of the enzyme ribulose 1,5-

bisphosphate carboxylase/oxygenase (Rubisco) within the Calvin-Benson cycle. J_{max}^{25} is

related to the intrinsic properties of the thylakoid membrane, which corresponds to the

availability of the cytochrome b6f complex (Cty f) (Hikosaka and Terashima, 1995) to transport

electrons in order to produce chemical energy transfers such as ATP and NADPH. ATP and

67 NADPH are then used to drive the Calvin-Benson Cycle by reducing Rubisco into ribulose

68 bisphosphate (RuBP). On average about two electrons are needed to reduce one unit of Rubisco,

69 implying a constant ratio between J_{max}^{25} and V_{max}^{25}. Frequently, V_{max}^{25} and J_{max}^{25} are each

70 prescribed as a constant value for a given plant functional type (PFT) based on limited

71 measurements (Medlyn et al., 1999; Wullschleger, 1993). Owing to the fact that Rubisco and

72 Cty f are both rich in nitrogen, some studies derived V_{max}^{25} and J_{max}^{25} from a global

73 compilation of nitrogen traits in plants, assuming a linear relationship between Rubisco and

74 leaf nitrogen content per unit area (N_{area}) (Kattge et al., 2009; Walker et al., 2014). However,

75 accurately represented temporal and spatial variations in both V_{max}^{25} and J_{max}^{25} are still elusive

76 as a robust observational methodology to quantify the dynamics of N_{area} across large spatial

77 extents is lacking (Knyazikhin et al., 2013). Moreover, some studies have questioned the

78 efficacy of the nitrogen-based method because the relationship between N_{area} and Rubisco

79 varies temporally due to the dynamic allocation of N_{area} between photosynthetic and non-

80 photosynthetic components in leaves, particularly over a growing season (Croft et al., 2017;

81 Kalacska et al., 2015).

82

83 Recent research has drawn attention to the potential of using leaf chlorophyll content (Chl_{leaf})

84 as an alternative constraint on leaf photosynthetic capacities (Croft et al., 2015a, 2017; Houborg

85 et al., 2013; Koffi et al., 2015; Alton, 2017). Chlorophyll molecules located in light-harvesting-

86 complexes (LHCs) absorb photons, which are then transported to initiate specific redox

87 reactions of chlorophyll molecules in Photosystem II to donate electrons to the electron

88 transport chain (ETC). The concentration of Chl_{leaf} is related to the rate of photosynthesis

89   through its determining role in the instantaneous electron transport rate (J) (Porcar-Castell et

90   al., 2014). As Chl_{leaf} is a nitrogen rich pigment, Chl_{leaf}, Rubisco and Cty f are linearly related

91   to each other according to their common correlations to the leaf photosynthetic nitrogen pool

92   (Evans, 1989a; Hikosaka and Terashima, 1996; Terashima and Evans, 1988). Recent research

93   has demonstrated that it is possible to model J_{max}^{25} and V_{max}^{25} from Chl_{leaf} using simple linear

94   equations (Houborg et al., 2013; Croft et al., 2017). This potential role of Chl_{leaf} as a proxy for

95   photosynthetic capacity has important implications for improved modelling at regional to

96   global scales, through the ability of estimating Chl_{leaf} from remotely sensed data, using

97   empirical (Croft et al., 2014a; Gitelson et al., 2005; Wu et al., 2008) and physically-based

98   models (Croft et al., 2013; Croft et al., 2015b; Houborg et al., 2015a; Zhang et al., 2007).

99   Satellite-derived Chl_{leaf} will provide an accurate, achievable way of quantifying J_{max}^{25} and

100   V_{max}^{25} in a temporally and spatially explicit manner.

101

102   Based on the assumptions above, Houborg et al. (2013) proposed a framework to incorporate

103   measured or satellite-derived Chl_{leaf} into TBMs by building universal Chl_{leaf}– V_{max}^{25}

104   relationships for C3 and C4 plants. Their inclusion of Chl_{leaf} into a TBM helped the GPP

105   simulations to better capture the daily and seasonal variations of observed fluxes over a corn

106   field. Beyond that, limited work has been done to incorporate Chl_{leaf} in TBMs, except for works

107   that have related Chl_{leaf} to vegetation productivity using empirical light use efficiency (LUE)

108   approaches (Croft et al., 2015a; Gitelson et al., 2006; Houborg et al., 2011). As forests account

109   for 50% of the global GPP (Pan et al., 2013) and 45% of the global ET (Oki and Kanae, 2006),

110   there is a growing interest in exploring the potential to use Chl_{leaf}–V_{max}^{25} relationship in forests

111   to improve the prediction of carbon and water fluxes in these areas.

112

113   The complex structures of forest canopies present greater challenges in the upscaling process

114   than for homogenous croplands. Canopy architecture leads to an uneven distribution of solar

115   irradiance from the sunlit top of trees to the shaded interior of a canopy. Values of N_{area} are

116   larger in the sunlit part of the canopy than in shaded leaves, with N_{area} declining from the top

117   to the bottom of a canopy, mimicking the gradient of long-term radiation distribution (Field,

118   1983; Hirose and Werger, 1987; Niinemets, 1997; Warren and Adams, 2001). Along with the

119   changes in N_{area}, the abundance of the nitrogen-rich photosynthetic components -- Rubisco and

120   Cty f -- is reported to be highly correlated to N_{area} and vary from the top to the bottom of the

121   canopy in proportion with N_{area} (Evans, 1989a; Sage et al., 1987). However, Chl_{leaf} is reported

122   to be largely unrelated to the N_{area} gradient and is almost uniform for leaves under various light

123   environments (Anderson et al., 1988; Iio et al., 2005; Lambers et al., 2008; Lichtenthaler et al.,

124   2007; Terashima and Evans, 1988; Walters, 2005), although some studies show a slight

125   chlorophyll gradient (Demarez et al., 1999; Yang et al., 2016; Zhang et al., 2007). These trends

126   lead to a substantially higher Chl_{leaf} : N_{area} ratio in shaded conditions than in full sunlight, which

127   imposes variations on the Chl_{leaf}–V_{max}^{25} relationships inside a canopy. This phenomenon has

128   been attributed to an optimal nitrogen allocation in plants, to maximise the overall productivity

129   of the canopy (Kull, 2002). Accordingly, for shaded leaves, relatively more nitrogen will be

130   allocated to chlorophyll in order to harvest photons, while for sunlit leaves, relatively more

131   nitrogen will be invested in Rubisco and Cty f to accelerate dark reactions (Evans, 1989b;

132   Hikosaka, 2014; Hikosaka and Terashima, 1996).

133

134 In this study, a TBM incorporating a two-leaf upscaling scheme is used to estimate GPP and

135 ET within a deciduous forest, across two growing seasons. The two-leaf scheme separates a

136 canopy into groups -- sunlit leaves and shaded leaves -- based on the first-order features of

137 instantaneous solar irradiance on leaves (Chen et al., 1999; Norman, 1982; Sinclair et al., 1976).

138 It is a robust description of the complex leaf light environment in canopies and has been proven

139 to be more capable of simulating GPP and ET variations than the commonly used big-leaf

140 scheme (Chen et al., 1999; De Pury and Farquhar, 1997; Luo et al., in review). The two-leaf

141 scheme delivers an available and potential tool to account for the variations in the Chl_{leaf}–V_{max}^{25}

142 relationship in a complex forest canopy, as well as for other physiological traits affected by the

143 light environment. Using intensive leaf-level and canopy-level measurements at a temperate

144 broadleaf forest, the specific objectives of this study are to:

145 1) investigate the improvements in GPP and ET simulations from a two-leaf TBM that uses

146 Chl_{leaf} to constrain V_{max}^{25};

147 2) evaluate the differences in the Chl_{leaf}–V_{max}^{25} relationship, and other physiological traits,

148 between sunlit and shaded leaves.

149

150 **2.0 Materials and methods**

151 **2.1 Site profile**

152 The Borden Forest Research Station is a mixed temperate forest site located in southern Ontario,

153 Canada (44°19'N, 79°56'W) (Froelich et al., 2015). It lies within an ecotone that extends across

154 eastern North America between 44 and 47°N and contains both southern temperate species and

155 northern boreal species. The vegetation at the Borden site is dominated by red maple (*Acer*

156 *rubrum*), eastern white pine (*Pinus strobus*), large-tooth and trembling aspen (*Populus*

157 *grandidentata* and *Populus tremuloides*) and white ash (*Fraxinus americana* (Lee et al., 1999;

158 Teklemariam et al., 2009). The fetch of largely uninterrupted forest extends to distances of 1.5–

159 4 km in the southeastern and southwestern quadrants, and to 1 km in the northeastern direction.

160 The northwestern fetch contains a white pine plantation and was not included in the footprint

161 of eddy-covariance (EC) flux calculations   at the site (Froelich et al., 2015). The soil type is

162 sandy loam (Gonsamo et al., 2015). From 2008 to 2013, the average temperature was 8.64℃,

163 precipitation was 808 mm/year and average daytime solar irradiance was 301 W/m$_2$.

164

165 **2.2 Field measurements**

166 Four dominant C3 broadleaf species (red maple, trembling aspen, large-tooth aspen and white

167 ash) were sampled during the growing seasons of 2013, 2014 and 2015. Foliar chlorophyll was

168 measured every 7 to 15 days from five leaf samples per species taken from top-of-canopy

169 branches accessed directly from the 44 m flux tower. Branches were tagged to ensure repeatable

170 sampling throughout the season, and the leaf samples were kept in cool, dark conditions during

171 transport back to a laboratory for analysis. Leaf chlorophyll was extracted using *N,N-*

172 *dimethylformamide*, and was analysed using a Shimadzu UV-1700 Spectrophotometer, with

173 extinction coefficients specified by Wellburn (1994).

174

175 Leaf gas exchange measurements were made on the same days as chlorophyll sampling, using

176 a LI- 6400XT portable infrared gas analyser (LI-COR Inc., Lincoln, NE, USA). CO$_2$ response

177 curves (A-Ci curve) of the leaves on the tagged branches were measured under an artificial

178 saturated light source of 1800 μmol photons m-2s-1 and stepwise ambient CO_2 concentrations

179 of 400, 200, 100, 50, 400, 400, 600, 800, 1000, 1200, 1500, 1800 ppmv. $V_{max}^{25}{}_{\_0}$ and $J_{max}^{25}{}_{\_0}$,

180 the V_{max}^{25} and J_{max}^{25} of the leaves at the top of the canopy, were calculated from the A-Ci

181 curves using a curve-fitting tool developed by Kevin Tu (www.landflux.org) following Ethier

182 and Livingston (2004) and then normalised to 25 °C (Sharkey et al., 2007).

183

184 Canopy structural parameters were also collected at 10 m intervals on the same days along a

185 100 m transect, extending from the flux tower in a North-South orientation. Effective LAI (L_e)

186 values were obtained using the LAI-2000 plant canopy analyser (Li-Cor, Lincoln, NE, USA),

187 while the element clumping index (Ω_E) was measured using the TRAC (Tracing Radiation and

188 Architecture of Canopies) instrument (Chen and Cihlar, 1995). The true LAI time sequences

189 were then calculated as follows (Chen et al., 1999):

$$LAI = [(1 - \alpha)L_e \gamma_E]/\Omega_E \qquad (1)$$

191 where α is the ratio of woody area to total area and γ_E is the ratio of needle area to shoot area.

192 The ratio of woody area to total area (α = 0.17) (Croft et al, 2015a) accounts for the interception

193 of radiation by branches and tree trunks that results in artificially high LAI values, Ω_E is set

194 at 0.95 based on the TRAC measurements. For broadleaf species, individual leaves are

195 considered the foliage elements and γ_E is set at 1.

196

197 **2.3 Flux and meteorological measurements**

198 The eddy covariance measurements were made at the height of 33 m using a sonic anemometer

199 (K-Type, Applied Technologies Inc., USA) coupled with a closed-path infrared gas analyzer

200 (IRGA, model LI-6262, LI-COR Biosciences, USA) which is located in a temperature-

201 controlled hut at the base of the tower. Both the IRGA and anemometer are operated at 10 Hz.

202 High frequency eddy covariance fluxes were processed and aggregated into half-hourly fluxes

203 using the method described in Froelich et al. (2015).

204 The half-hourly net ecosystem exchange (NEE, μmol m$_{-2}$s$_{-1}$) is calculated as $-(F_c+S_c)$, where

205 F_c is the covariance between vertical wind velocity (w') and atmospheric CO_2 concentration

206 (c'). S_c is the rate of change of CO_2 storage per unit ground area in the air layer below the EC

207 sensors. F_c was calculated from the WPL(Webb-Pearman-Leuning)-corrected vertical turbulent

208 transport of the CO_2 mole fraction as $F_c = \rho_a \overline{w'c'_{WPL}}/M_a$, where the WPL accounts for

209 density effects due to water vapor fluctuations (Webb et al., 1980), ρ_a is the density of air and

210 M_a is the molecular weight of dry air. The storage change S_c was estimated as $S_c =$

211 $\int_0^{Z_{ec}} \frac{\Delta CO_2}{\Delta t} dz$, where Z_{ec} is the height of the EC sensors at 33m and t refers to time. Other terms

212 such as horizontal advection are assumed to be negligible. NEE data were then filtered during

213 periods of low turbulence (Staebler and Fitzjarrald, 2004) and when winds were from the

214 direction of the short fetch (i.e. wind direction was >285° or <20°) (Froelich et al., 2015). A

215 change point detection method (Barr et al., 2013) was used to derive the friction velocity

216 threshold (u*) to identify periods suitable for the application of the eddy covariance method to

217 calculate fluxes. Gaps in the NEE data were filled using the method of Barr et al. (2004). During

218 nights or cold periods respiration (RE) was simply computed as $RE = NEE$, while during

219 warm periods or in cases of data gaps, RE was estimated using an empirical model based on

220 air and soil temperature (Froelich et al., 2015). Half-hourly GPP was then calculated as $GPP =$

221   *NEE + RE*; gaps in GPP were filled with an empirical model based on PAR (Barr et al., 2004;

222   Froelich et al., 2015).

224   In conjunction with the CO_2 flux measurements, the EC system also measured the latent heat

225   flux (LE, W m-2) as $LE = L\rho_a \overline{w'q'_{WPL}}$, where L is the latent heat of vaporization (kJ g-1), ρ_a

226   is the density of air (kg m-3) and $\overline{w'q'_{WPL}}$ is the WPL-corrected covariance between the

227   vertical wind velocity and atmospheric water vapor mixing ratios (m s-1 mol H_2O mol-1 air).

228   (Froelich et al., 2015; Teklemariam et al., 2009). Gaps in the LE measurements were not filled.

230   Several half-hourly auxiliary microclimate variables were also collected at the site to initialize

231   and force the TBM. Wind speed (m s-1) and wind direction were measured by the sonic

232   anemometer mounted at the height of 33 m. Continuous air temperature (°C) and relative

233   humidity (%) were measured at various heights, but the 33 meter data were selected as model

234   inputs. Incoming solar irradiance on the canopy was measured at the top of the flux tower

235   (Froelich et al., 2015). Soil moisture (m3 m-3) measured at the depth of 5 cm to 30 cm was used.

236   Precipitation data (mm h-1) were obtained from the nearest Environment Canada weather

237   station that has hourly rainfall records (ID: Borden AWO), which is approximately 5.2 km away.

239   **2.4 Terrestrial biophysical model**

240   The Boreal Ecosystem Productivity Simulator (BEPS) is a two-leaf enzyme-kinetic model

241   initially developed to estimate the carbon uptake and the water cycle of boreal ecosystems

242   (Chen et al., 1999; Liu et al., 2003). It has been substantially upgraded since its original release

243   to simulate carbon and water fluxes at an hourly time step over various PFTs (Chen et al., 2007;

244   Ju et al., 2006). Several inter-model comparisons and site-level validations have shown that

245   BEPS can produce reliable GPP and ET estimates (Amthor et al., 2001; Potter et al., 2001;

246   Grant et al., 2006; Gonsamo et al., 2013). The modules related to the utilization of Chl$_{leaf}$ in

247   BEPS are described in the following subsections.

248

249   **2.4.1 Separation of sunlit and shaded leaves.**

250   The two-leaf scheme is an abstraction of the instantaneous radiation regime in canopies. Leaves

251   are separated into sunlit leaves and shaded leaves based on illumination and canopy geometry.

252   Sunlit leaves tend to be light saturated because they receive both direct and diffuse solar

253   radiation, while shaded leaves only receive diffuse radiation (Appendix A). The values of

254   LAI_{sunlit} and LAI_{shaded} are calculated following the stratification scheme of Norman (1982)

255   and Chen et al. (1999):

$$LAI_{sunlit} = 2\cos\theta(1 - \exp(-0.5\Omega LAI_{tot}/\cos\theta)) \qquad (2)$$

$$LAI_{shaded} = LAI_{tot} - LAI_{sunlit} \qquad (3)$$

258   where θ is the solar zenith angle, LAI_{tot} is the total leaf area index of the canopy, and Ω is

259   the clumping index of this site, where $\Omega = \Omega_E/\gamma_E$.

260

261   **2.4.2 Derivation of V_{max}^{25} and J_{max}^{25} for sunlit and shaded leaves**

262   In BEPS, $V_{max\_0}^{25}$ is the input parameter to quantify the leaf photosynthetic capacity. The V_{max}^{25}

263   values for sunlit and shaded leaves are each derived respectively based on the $V_{max\_0}^{25}$ value,

264   the vertical nitrogen profile of the canopy, the fraction of sunlit and shaded leaves and (Chen

265   et al., 2012).

266   Leaf nitrogen content per unit leaf area $N(L)$ (g m-2) generally decreases exponentially from

267   the top to the bottom in a canopy following the long-term radiation distribution in the canopy

268   (Equation 4):

269    $$N(L) = N_0 e^{-k_n L} \qquad (4)$$

270   where the extinction coefficient $k_n = 0.3$ (De Pury and Farquhar, 1997), N_0 is the nitrogen

271   content of leaves at the top-of-canopy, and L is the canopy depth expressed as LAI from the

272   top to a given height. V_{max}^{25} is proportional to the leaf nitrogen content, and therefore it could

273   be expressed as:

274    $$V_{max}^{25}(L) = V_{max\_0}^{25} \chi_n N(L) \qquad (5)$$

275   where $V_{max\_0}^{25}$ is the V_{max}^{25} of leaves at the top-of-canopy, and χ_n (m2 g-1) quantifies the

276   relative change of V_{max}^{25} to the leaf nitrogen content in the canopy, while $N(L)$ has the unit of

277   g/m2. The value of χ_n , the mean value of N$_{area}$ and its standard deviation, and the standard

278   deviation of V_{max}^{25} are provided for each PFT (Chen et al., 2012; Kattge et al., 2009); we have

279   only used the values for deciduous broadleaf forests in this study. Since we do not have records

280   specifically for N_0, N_0 is regarded as the sum of the mean N$_{area}$ and its standard deviation,

281   which are provided by Kattge et al. (2009). Using Equation 4 and 5 and our estimated N_0, we

282   can quantify the vertical patterns of V_{max}^{25} in the canopy.

283

284   The fractions of sunlit (f$_{sun}$) and shaded leaves (f$_{sh}$)in the canopy change with the canopy depth:

285    $$f_{sun}(L) = \Omega e^{-kL} \qquad (6)$$

286    $$f_{sh}(L) = 1 - \Omega e^{-kL} \qquad (7)$$

287   where $k = G(\theta)\Omega/\cos\theta$. The projection coefficient of the canopy, $G(\theta)$, is taken as 0.5

288   assuming a spherical leaf angle distribution. We assume that V_{max}^{25} of a representative sunlit

289   or shaded leaf is equal to the mean V_{max}^{25} value of the sunlit or shaded leaf group. Therefore,

290   the V_{max}^{25} of a representative sunlit or shaded leaf is expressed through the following

291   integrations:

292   $V_{max\_sunlit}^{25} = \dfrac{\int_0^L V_{max\_0}^{25}\chi_n N(L)f_{sun}(L)dL}{\int_0^L f_{sun}(L)dL} = V_{max\_0}^{25}\chi_n N_0 \dfrac{\int_0^L e^{-k_n L}\Omega e^{-kL}dL}{\int_0^L \Omega e^{-kL}dL} =$

293   $V_{max\_0}^{25}\chi_n N_0 \dfrac{k[1-e^{-(k_n+k)L}]}{(k_n+k)(1-e^{-kL})}$ (8)

294

295   $V_{max\_shaded}^{25} = \dfrac{\int_0^L V_{max\_0}^{25}\chi_n N(L)f_{sh}(L)dL}{\int_0^L f_{sh}(L)dL} = V_{max\_0}^{25}\chi_n N_0 \dfrac{\int_0^L e^{-k_n L}(1-\Omega e^{-kL})dL}{\int_0^L (1-\Omega e^{-kL})dL} =$

296   $V_{max\_0}^{25}\chi_n N_0 \dfrac{\frac{1}{k_n}(1-e^{-k_n L})-\frac{\Omega}{k+k_n}[1-e^{-(k_n+k)L}]}{L-2\cos\theta(1-e^{-kL})}$ (9)

297

298   Several methods for estimating $V_{max\_0}^{25}$ are described in Section 2.5. J_{max}^{25} for sunlit and

299   shaded leaves are subsequently obtained using the $V_{max}^{25}:J_{max}^{25}$ built on our in-situ

300   measurements (see Section 2.5).

301

302   **2.4.3 Simulation of GPP and ET**

303   BEPS calculates the instantaneous GPP as the sum of the photosynthesis from the sunlit leaves

304   and the shaded leaves (Equation 10). Within each sunlit and shaded leaf group, all leaves are

305   assumed to have the same physiological features; photosynthesis of a leaf group is then

306   predicted using one representative leaf multiplied by LAI.

307      $GPP = A_{sunlit} \times LAI_{sunlit} + A_{shaded} \times LAI_{shaded}$ (10)

308   where A_{sunlit} and A_{shaded} are the instantaneous photosynthetic rates of a representative

309 sunlit leaf and a representative shaded leaf, respectively. Following the Farquhar biochemical

310 model, the instantaneous leaf photosynthetic rate in BEPS (Chen et al., 1999) is described as:

311
$$A = \min(W_c, W_j) - R_d \tag{11}$$

312 where W_c is the rate of gross photosynthesis (µmol m-2s-1) when RuBP

313 carboxylase/oxygenase is saturated, and W_j is the photosynthetic rate when RuBP-

314 regeneration is limited by electron transport. R_d is the dark respiration rate of CO2 exchange.

315
$$W_C = V_{max} \frac{C_i - \Gamma}{C_i + K} \tag{12}$$

316
$$W_j = J \frac{C_i - \Gamma}{4C_i + 8K} \tag{13}$$

317

318
$$R_d = 0.015 V_{max} \tag{14}$$

319 where V_{max} is the maximum carboxylation rate (µmol m-2s-1) acquired from the prescribed

320 V_{max}^{25} and a temperature dependent function (Sharkey et al., 2007), J is the electron transport

321 rate (µmol m-2s-1). C_i is the intercellular CO2 concentration (µmol mol-1), and Γ is the CO2

322 compensation point in the absence of dark respiration (µmol mol-1), K is a function of Rubisco

323 enzyme kinetics described as $K_c/(1 + O_i/K_o)$, where K_c and K_o are Michaelis–Menten

324 constants for CO2 (µmol mol-1) and O2 (mmol mol-1) and O_i is the intercellular oxygen

325 concentration (mmol mol-1). The electron transport rate, J, is a function of the incoming

326 photosynthetic photon flux density (PPFD in µmol m-2s-1) and the maximum electron transport

327 (J_{max}):

328
$$J = J_{max} PPFD / (PPFD + 2.1 J_{max}) \tag{15}$$

329 Following a revised Ball-Woodrow-Berry equation (Ju et al., 2006), leaf stomatal

330 conductance is quantified as:

331

$$g_s = f_w \left(\frac{mA \cdot RH}{C_s} \right) + g_0 \qquad (16)$$

333   where m is the dimensionless Ball-Woodrow-Berry coefficient set as 8, RH is the relative

334   humidity (%), C_s is the CO_2 concentration on the leaf surface, g_0 is the minimum

335   conductance during the night, and A is the rate of photosynthesis (μmol m-2s-1) of the

336   representative sunlit or shaded leaf. The added f_w variable is noted as the soil water stress

337   factor (Appendix B).

338   After obtaining g_s, leaf-level transpiration is calculated by employing the Penman-Monteith

339   equation in BEPS (Chen et al., 2007):

$$T = \frac{\Delta(R_n - G) + \rho c_p VPD g_v}{\Delta + \left(1 + \frac{g_v}{g_s}\right)\gamma} \times \frac{1}{\lambda} \qquad (17)$$

341   where λ is the latent heat of water (J kg-1), R_n is the instantaneous net radiation on the leaf

342   surface (W/m-2) ((Appendix A), G is the heat storage of the leaf which is a minimum close to

343   0 (W/m-2), ρ is the density of air (kg m-3), c_p is the specific heat of air (J kg-1 °C-1), VPD is

344   the vapor pressure deficit on the surface of a leaf (kPa), γ is the psychrometric constant

345   (kPa °C-1), g_v is the leaf boundary-layer resistance to water vapor (m s-1), and Δ is the

346   derivative of saturated vapor pressure with respect to the air temperature (kPa °C-1). The leaf-

347   level transpiration (mm s-1) is upscaled to the canopy-level transpiration following an

348   analogous protocol to the GPP upscaling.

$$T = T_{sunlit} \times LAI_{sunlit} + T_{shaded} \times LAI_{shaded} \qquad (18)$$

350   where T_{sunlit} is the transpiration from a sunlit leaf and T_{shaded} is the transpiration from a

351   shaded leaf.

352   In addition to transpiration, BEPS also simulates evaporation from soil and from wet leaves

353   (Chen et al., 2007). These processes are not regulated by stomata and therefore are less likely

354   to be affected by the improvement in V_{max}^{25} parameterization.

355

356   **2.5 Modelling treatments**

357   Empirical equations were developed to relate Chl$_{leaf}$ to $V_{max\_0}^{25}$ and $J_{max\_0}^{25}$, based on field

358   measurements (Croft et al., 2017) and were incorporated into BEPS for the purpose of

359   improving GPP and ET simulations. In order to evaluate the improvements associated with

360   utilising Chl$_{leaf}$ (Case 4), we used three commonly employed $V_{max\_0}^{25}$ treatments as reference

361   cases (Case 1,2 and 3).

362

363   **Case 1:** constant $V_{max\_0}^{25}$. Groenendijk et al. (2011) assimilated eddy covariance measurements

364   from Fluxnet into an inverse model of photosynthesis and transpiration to derive site-specific

365   V_{max}^{25} and PFT-specific V_{max}^{25}. Several BEPS studies have successfully used this set of V_{max}^{25}

366   values for site-level GPP and ET simulations (Gonsamo et al., 2013; Chen et al., 2016; Luo et

367   al., 2017, in review).

368   In this case, we used the value of 62 μmol m-2 s-1 for temperate deciduous broadleaf forest from

369   Groenendijk et al. (2011) as the constant $V_{max\_0}^{25}$ at the Borden Forest site. This value is

370   comparable to another commonly cited value of 57.7 μmol m-2 s-1 for deciduous broadleaf

371   forests reported by Kattge et al. (2009).

372

373   **Case 2:** LAI-based $V_{max\_0}^{25}$. Some studies have found that seasonal patterns of V_{max}^{25} follow

374   the seasonal patterns of LAI. We used a scheme developed by Ryu et al. (2011) to calculate

375     $V_{max\_0}^{25}$ on any given day during the growing season:

376 $$V_{max\_0}^{25} = aV_{max\_ref}^{25} + (1-a)V_{max\_ref}^{25} \frac{L_c - L_{min}}{L_{max} - L_{min}} \tag{19}$$

377   where L_{max}, L_{min} and L_c are maximum, minimum and current LAI values over the year.

378     $V_{max\_ref}^{25}$ is the value of maximum V_{max}^{25} during the growing season, which is regarded as 62

379   μmol m-2 s-1. The empirical variable a is set at 0.3 as in Ryu et al. (2011). The ratio component

380     $\frac{L_c - L_{min}}{L_{max} - L_{min}}$ ranges between 0 and 1.

381

382   **Case 3:** SLA-based $V_{max\_0}^{25}$. The specific leaf area (SLA) of leaves at the canopy top is used

383   in the Community Land Model version 4.0 (CLM4) to parameterize $V_{max\_0}^{25}$ (Thornton and

384   Zimmermann, 2007). In this case:

385 $$V_{max\_0}^{25} = N_{area} F_{LNR} F_{NR} \alpha_{R25} f(N) \tag{20}$$

386   where N_{area} is the area-based leaf nitrogen concentration (g N m-2), $F_{LNR} = 0.09$ is the

387   fraction of leaf nitrogen in Rubisco (g N in Rubisco g-1 N) for temperate broadleaf deciduous

388   trees, $F_{NR} = 7.16$ is the mass ratio of total Rubisco molecular mass to nitrogen in Rubisco (g

389   Rubisco g-1 N in Rubisco), and $\alpha_{R25} = 60$ is the specific activity of Rubisco (μmol CO_2 g-1

390   Rubisco s-1). A scaling factor, $f(N) = 0.64$, represents the effects of N limitation. N_{area} is

391   calculated from mass-based leaf N concentration and SLA.

392 $$N_{area} = \frac{1}{CN_L SLA} \tag{21}$$

393   where $CN_L = 25$ is the leaf carbon-to-nitrogen ratio (g C g-1 N) for broadleaf trees and SLA

394   is specific leaf area (m2 g-1 C).

395

396   **Case 4:** Chlleaf-based $V_{max\_0}^{25}$. A straightforward way to implement Chlleaf into TBMs is through

397 a robust relationship between Chl_{leaf} and the photosynthetic parameters (i.e. V_{max}^{25} and J_{max}^{25}).

398 Croft et al. (2017) found a significant linear relationship between Chl_{leaf} and $V_{max\_0}^{25}$ ($r^2=0.76$,

399 $p<0.001$) for the four deciduous species at the Borden site with an intercept close to zero
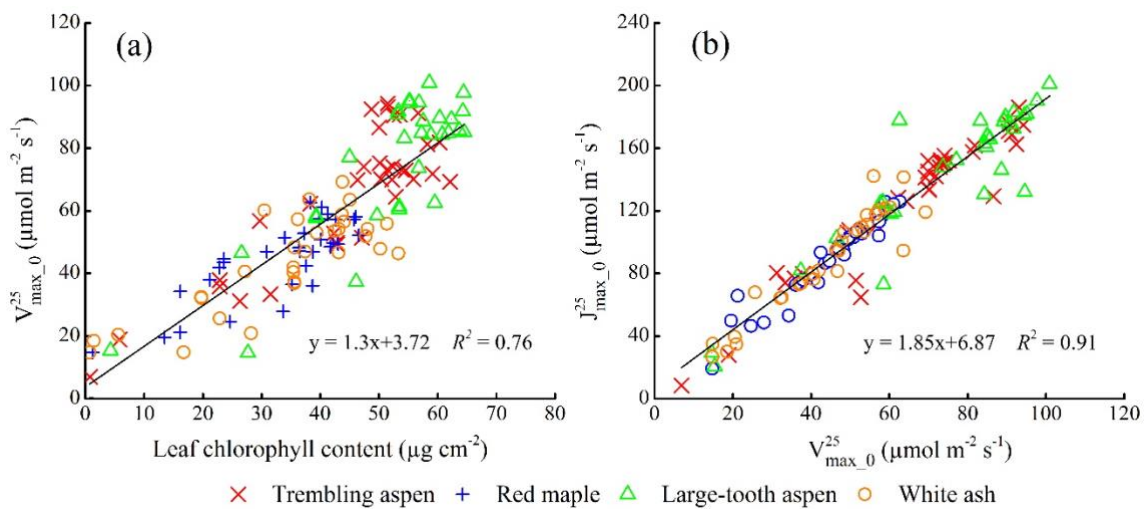
400 (Equation 22 and 23).

401
$$V_{max\_0}^{25} = 1.3 \times Chl_{leaf} + 3.72 \tag{22}$$

402

403
$$J_{max\_0}^{25} = 1.85 \times V_{max\_0}^{25} + 6.87 \tag{23}$$

404 For leaves at the top of the canopy, an increase of 1 μg cm-2 of Chl_{leaf} corresponds to 1.3 μmol

405 m-2 s-1 in $V_{max\_0}^{25}$. $V_{max\_0}^{25}$ and $J_{max\_0}^{25}$ are significantly related ($r^2=0.91$, $p<0.001$) by an

406 empirical equation across four species (Figure 1).

407

408

409 **Figure 1.** Scatter plots of the measured leaf-level physiological parameters of C3 broadleaf

410 leaves at the top of canopy at the Borden site in 2014 and 2015. (a) $V_{max\_0}^{25}$ versus Chl_{leaf};

411 (b) $J_{max\_0}^{25}$ versus $V_{max\_0}^{25}$. Source: Croft et al., 2017.

412

413 While the ranges of Chl_{leaf}, $V_{max\_0}^{25}$ and $J_{max\_0}^{25}$ each differ among the four species, the linear

414   equations in Figure 1 fit the data points consistently, implying that it is reasonable to use a

415   single equation to link Chl_{leaf} and $V_{max\_0}^{25}$ for broadleaf species. These two equations were used

416   to incorporate Chl_{leaf} into BEPS in Case 4.

417

418   **3. Results**

419   **3.1 Leaf traits and canopy fluxes**

420   Figure 2 shows the variations of Chl_{leaf}, LAI and SLA that are used to constrain $V_{max\_0}^{25}$ in the

421   four modelling cases (Figure 2a), along with simulated V_{max}^{25} and canopy flux measurements

422   (Figure 2b) across two growing seasons. Chl_{leaf}, LAI and SLA were measured every 7-15 days

423   during the two growing seasons; values between the sampling dates were determined by linear

424   interpolation. The Chl_{leaf} and SLA values were calculated based on the weighted composition

425   of the major tree species at the Borden Forest (Teklemariam et al., 2009).
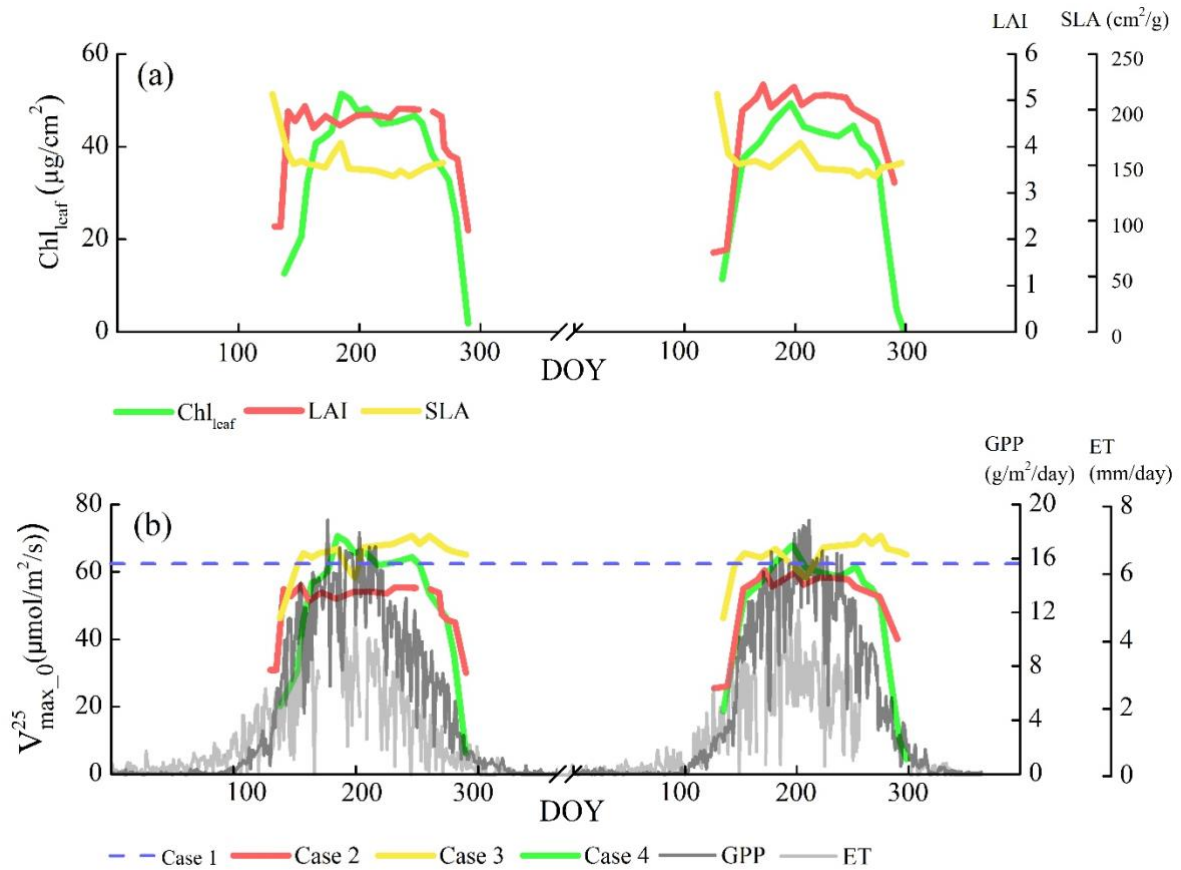
Figure 2. Seasonal variations of (a) Chl_{leaf}, leaf area index (LAI), specific leaf area (SLA),

and; (b) simulated $V_{max\_0}^{25}$ for each modelling scenario where: Case 1 (a constant $V_{max\_0}^{25}$),

Case 2 (LAI-based $V_{max\_0}^{25}$), Case 3 (SLA-based $V_{max\_0}^{25}$) and Case 4 (Chl_{leaf}-based $V_{max\_0}^{25}$),

alongside GPP and ET tower measurements, during 2013 and 2014 at the Borden Forest field

site.

In 2013 and 2014, Chl_{leaf} accumulated slowly, beginning in early May, reached its peak in July,

with values ranging from 0.6 to 51.4 µg cm-2. In contrast, leaves became fully expanded in a

shorter time-frame (over 2 weeks in early-mid May), giving a steeper gradient in the early

growing season LAI values. SLA decreased promptly at the beginning of growing seasons and

stayed relatively constant from May to October. At the end of the growing season, the

438 breakdown of chlorophyll began to exceed production in late August, while leaf fall did not

439 begin until October (Croft et al., 2014).

440

441 Among the four cases, the simulated Chl$_{leaf}$-based $V^{25}_{max\_0}$ (Case 4) appears to most closely

442 follow the seasonal variations in measured GPP and ET (Figure 2b). In the modelled scenarios,

443 simulated $V^{25}_{max\_0}$ ranges from: Case 2 - 30.1 to 60.5 μmol m-2 s-1; Case 3 - 35 to 70.2 μmol

444 m-2 s-1; and Case 4 - 4.4 to 70.6 μmol m-2 s-1. Values of $V^{25}_{max\_0}$ from these modelling cases are

445 used in BEPS to simulate GPP and ET over two growing seasons at the Borden Forest.

446

447 **3.2   Validation of the GPP and ET estimates from different $V^{25}_{max\_0}$ constraints**

448 The simulated GPP and ET results are shown for the four different modelling cases, in order to

449 investigate the effects of the different biophysical constraints on $V^{25}_{max\_0}$. Figure 3 shows linear

450 regressions between the hourly measured fluxes and the hourly estimated fluxes from BEPS.

451
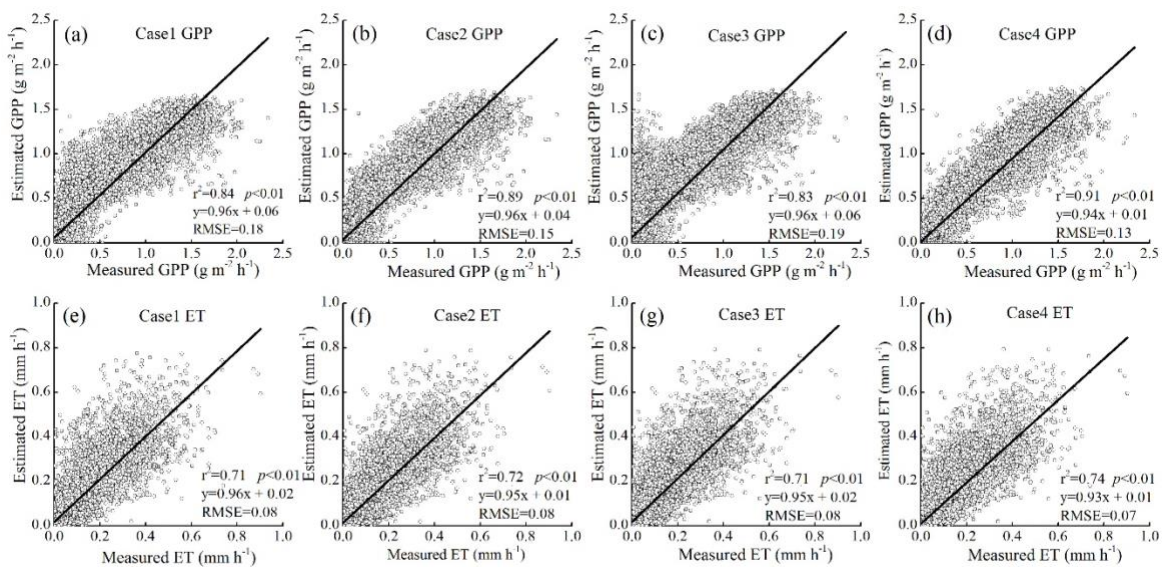
452

453   **Figure 3.** Scatter plots of the predicted and measured fluxes of 2013-2014 at the Borden site.

22

454　　　(a) to (d) refer to the GPP validation in Case 1 (a constant $V_{max\_0}^{25}$), Case 2 (LAI-based

455　　　$V_{max\_0}^{25}$), Case 3 (SLA-based $V_{max\_0}^{25}$) and Case 4 (Chl$_{leaf}$-based $V_{max\_0}^{25}$), respectively; (e) to

456　　　　　(h) refer to the ET validation in Case 1, Case 2, Case 3 and Case 4, respectively.

457

458　　Modelled results from Case 4 (Chl$_{leaf}$-based $V_{max\_0}^{25}$) show the strongest correlation ($r_2 = 0.91$)

459　　with measured GPP values, and the lowest RMSE of 0.13 g m$_{-2}$ h$_{-1}$ (Figure 3). The other three

460　　modelled scenarios reveal overestimated results at lower GPP values, which likely correspond

461　　to the start and the end of the growing season. Additionally, Case 1 (a constant $V_{max\_0}^{25}$) shows

462　　underestimations at higher measured GPP values. The total simulated annual GPP values are

463　　2123 g m$_{-2}$ y$_{-1}$, 1967 g m$_{-2}$ y$_{-1}$, 2124 g m$_{-2}$ y$_{-1}$ and 1729 g m$_{-2}$ y$_{-1}$ for Case 1 (a constant $V_{max\_0}^{25}$),

464　　Case 2 (LAI-based $V_{max\_0}^{25}$), Case 3 (SLA-based $V_{max\_0}^{25}$) and Case 4 (Chl$_{leaf}$-based $V_{max\_0}^{25}$),

465　　respectively, while the annual GPP obtained from flux-tower measurements is 1719 g m$_{-2}$ y$_{-1}$.

466　　The bias of the estimated annual GPP from Case 4 accounts for only 0.6% of observed annual

467　　GPP,　while the biases from Cases 1, 2 and 3 account for 23.5%, 14.4% and 23.6%,

468　　respectively.

469

470　　The Chl$_{leaf}$ -constrained $V_{max\_0}^{25}$ also produces the strongest relationship between estimated

471　　and measured ET ($r_2 = 0.74$; RMSE = 0.07 mm h$_{-1}$). As with the GPP results, the estimated

472　　annual ET for Case 4 of 362 mm y$_{-1}$ is closest to the measurement value of 370 mm y$_{-1}$, while

473　　the other annual ET results are 414 mm y$_{-1}$ (Case 1), 397 mm y$_{-1}$ (Case 2), 409 mm y$_{-1}$ (Case

474　　3). The bias of the estimated annual ET from Case 4 accounts for -2.2% of measured annual

475　　ET, while to the biases from Case 1, 2 and 3 account for 11.9%, 7.3% and 10.5% of the annual

476   observed ET. Overall, Case 4 is the most accurate scenario for simulating both total amount

477   and temporal variations of carbon and water fluxes.

478

479   **3.3 Seasonality of the improvements in estimated GPP and ET**

480   In order to investigate the seasonal variability in the improvements made to GPP and ET

481   estimations using Case 4 relative to Cases 1-3 (Figure 3), the monthly mean absolute errors

482   (MAEs) and the relative MAEs of the modelled fluxes are shown for the four cases (Figure 4). .

483

484
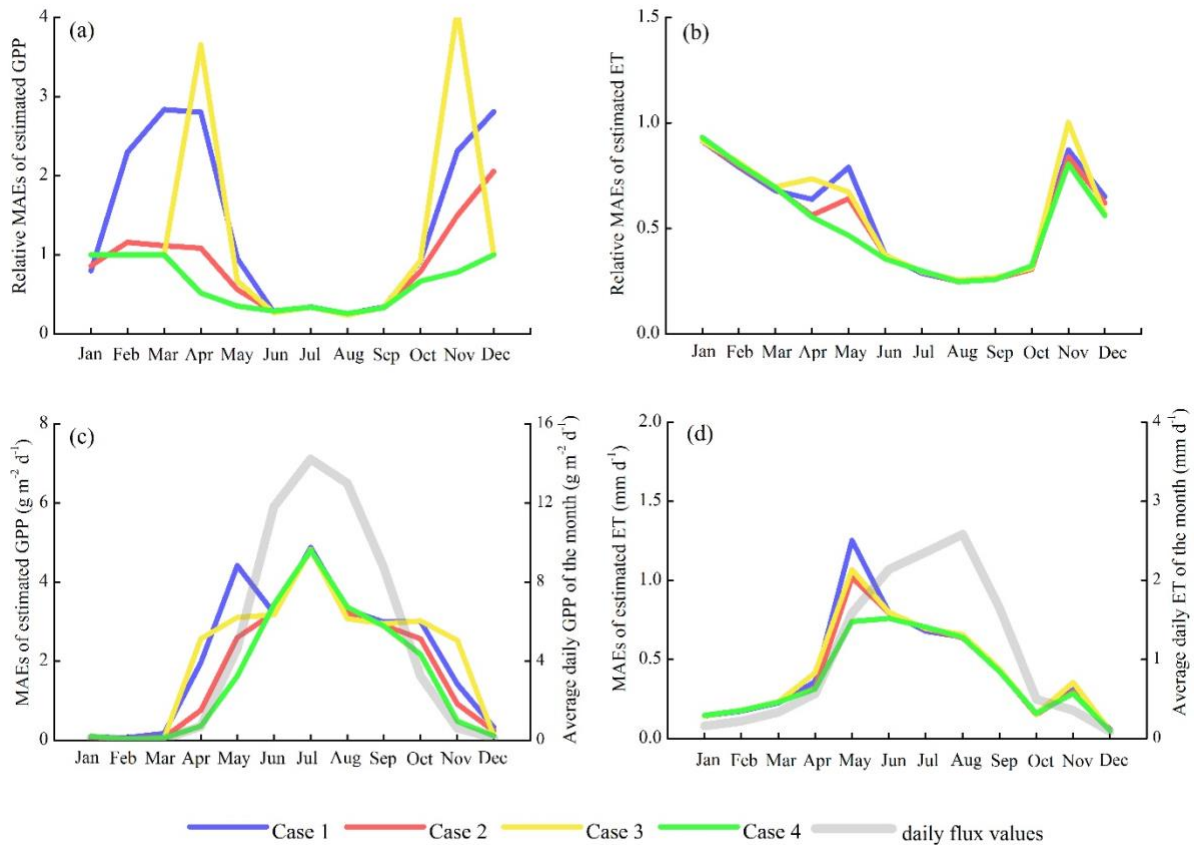
485

486   **Figure 4.** The monthly relative MAEs (a, b) and the MAEs (c, d) between the estimated and

487   measured daily fluxes in 2013-2014, under the four modelling cases. (a, c) GPP and (b, d) ET.

488   The relative MAEs are the division of MAEs by daily flux values.

489

490   Figure 4a and 4b shows that Case 4 introduces the smallest errors in most months for both GPP

491   and ET estimates. Other cases display larger MAEs and relative MAEs than Case 4, especially

492   at the beginning and end of the growing seasons. In Figures 4c and 4d, the average MAEs of

493   estimated GPP in spring (from April to June) of the four cases are 3.2 g m-2 d-1, 2.2 g m-2 d-1,

494   3.0 g m-2 d-1 and 1.8 g m-2 d-1 respectively; in autumn (from September to November), the

495   average MAEs of estimated GPP for the four cases are 2.4 g m-2 d-1, 2.1 g m-2 d-1, 2.8 g m-2 d-

496   1 and 1.8 g m-2 d-1, respectively. In the middle of the growing seasons, the improvements are

497   not pronounced since the V_{max}^{25} values derived from all cases are close to each other. The major

498   improvements in modelled ET also appear in spring (from April to June), where the MAEs are

499   reduced from 0.8 mm d-1 in Case 1, 0.7 mm d-1 in Case 2 and 0.8 mm d-1 in Case 3 to 0.6 mm

500   d-1 in Case 4. In fall (from September to November), small improvements on the order of 0.01

501   mm d-1 in MAEs are observed from Case 1, 2 and 3 to Case 4. From June to August, the ET

502   estimates show little differences among the four cases.

503

504   **3.4 Assessing the relative contribution of Chl$_{leaf}$ to modelled GPP and ET**

505   According to the modelling results, Chl$_{leaf}$ -V_{max}^{25} markedly improved the estimation of GPP

506   and ET during the transitional periods of the growing season. However, the improvement in

507   ET is not as great as the improvement in GPP (Figure 4). This decoupling effect of carbon and

508   water fluxes suggests that there are differences in the sensitivities of GPP and ET to the forcing

509   variables. In Figure 5, we explored the sensitivities of GPP and ET to five forcing variables of

25

510   BEPS: incoming solar radiation (R_s), air temperature (T_{air}), relative humidity (RH), LAI and

511   Chl_{leaf}. To assess the sensitivity of GPP and ET to certain variables, each variable was changed

512   by -20%, -10%, 10% and 20% stepwise to drive BEPS (Case 4), while all other variables

513   remained unchanged. The resulting changes in simulate GPP and ET were recorded and

514   analyzed.
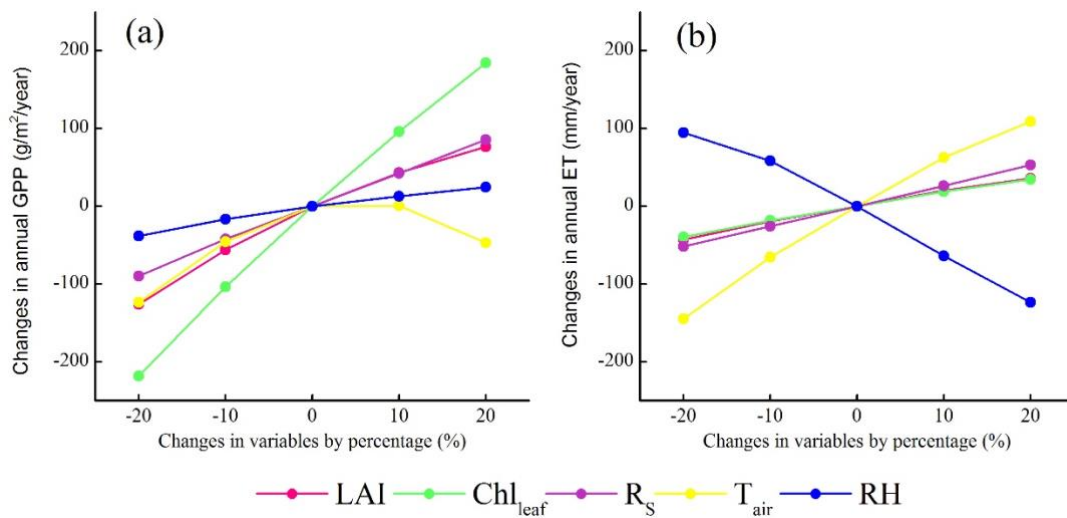
515

516   **Figure 5**. Sensitivity of GPP and ET to the incoming solar radiation (R_s), air temperature

517   (T_{air}), relative humidity (RH), LAI and Chl_{leaf} at the Borden site. (a) GPP; (b) ET.

518

519   Figure 5a shows that GPP is most sensitive to the changes in Chl_{leaf}. A 20% variation in Chl_{leaf}

520   leads to a change in annual GPP as large as 200 g m^{-2} y^{-1}. In addition to Chl_{leaf}, R_s and LAI are

521   linearly linked to GPP with similar order of importance. There is an optimal T_{air} range for GPP,

522   with higher or lower T_{air} damping the carbon assimilation rate. RH has the least influence on

523   GPP. In contrast, ET is most sensitive to the climatic variables, T_{air} and RH, whilevariables

524   used to describe the plant functional status (i.e. LAI and Chl_{leaf}) drive smaller changes in ET

525   (Figure 5b). As such, the variation in ET resulting from the changing Chl_{leaf} and LAI in spring

526   and autumn is overshadowed by the variation from changing temperature and humidity.

527   Consequently, ET is less improved than GPP by incorporating Chl$_{leaf}$ based V^{25}_{max} in the TBM.

528

529   **3.5 The impact of light environment within the canopy on leaf physiology**

530   This study incorporates Chl$_{leaf}$ into a two-leaf model to consider the complex light environment

531   in forests and the accompanying physiological traits of sunlit and shaded leaves. Light intensity

532   within the canopy affects the relative allocation of nitrogen between light-harvesting

533   chlorophyll molecules and Rubisco in the Calvin cycle. Consequently, it is important to

534   consider how this dynamic partitioning of nitrogen affects the integration of chlorophyll into

535   the two-leaf BEPS model, and how this partitioning impacts carbon and water exchange. Figure

536   6 shows the contrasting modelled solar irradiance for sunlit and shaded leaves over the two

537   growing seasons.

538
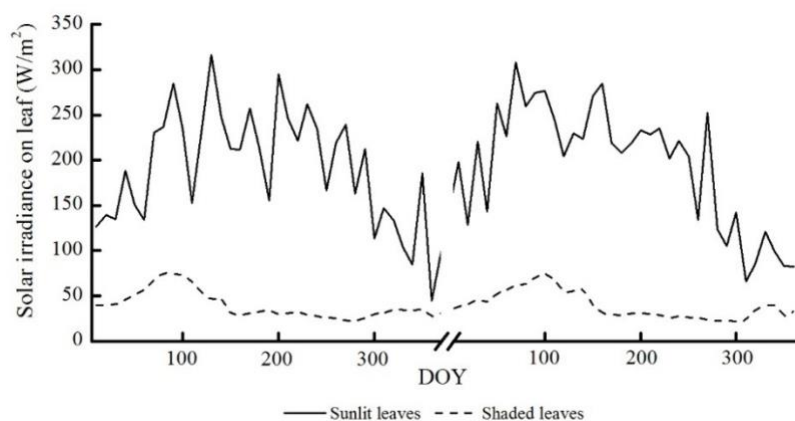
539

540   **Figure 6**. Seasonal patterns of the average daily incoming solar radiation (W/m$_2$) on sunlit

541   and shaded leaves simulated by BEPS in 2013 and 2014.

542   The daytime average solar radiation on sunlit leaves ranges from 105 to 316 W m$_{-2}$ from DOY

543   100 to DOY 300, with an average value of 216 W m$_{-2}$. In contrast, the solar irradiance on

544 shaded leaves ranges from 22 to 75 W m-2 in the same period, with an average of 36 W m-2.

545 This 6-fold difference in the light environment results in a different role of chlorophyll between

546 the sunlit and shaded leaves, as shown in Figure 7.
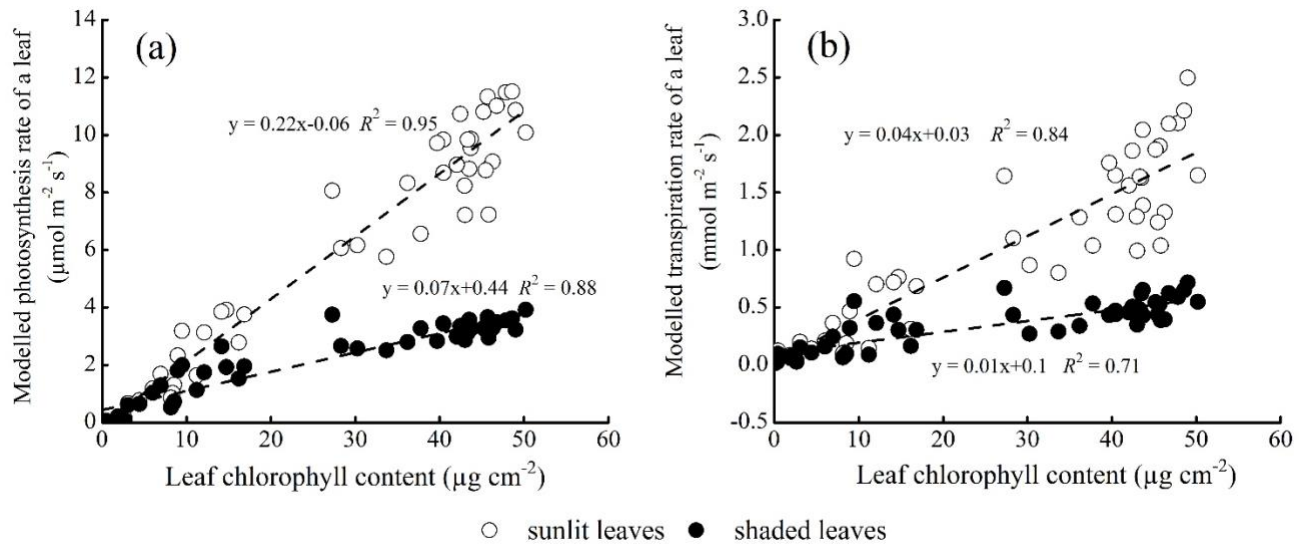

547

548 **Figure 7.** BEPS modelled leaf photosynthesis and transpiration rates and their relationship to

549 Chl$_{leaf}$. Sunlit (open dots) and shaded leaves (solid dots) are compared. Ten-day averages of

550 the modelled photosynthesis and transpiration rates in the growing seasons are used.

551

552 For modelled sunlit leaves, an increase of 1 μg cm-2 in Chl$_{leaf}$ increases the rate of

553 photosynthesis by 0.22 μmol m-2 s-1 and the rate of transpiration by 0.04 mmol m-2 s-1 in sunlit

554 leaves. In contrast, photosynthesis and transpiration of shaded leaves are less sensitive to

555 changes in Chl$_{leaf}$:a 1 μg cm-2 increase in Chl$_{leaf}$ leads to only a 0.07 μmol m-2 s-1 increase in

556 photosynthesis and a 0.01 mmol m-2 s-1 increase in transpiration of shaded leaves. Importantly,

557 Figure 7 suggests that chlorophyll plays a lesser role in determining GPP and ET in shaded

558 leaves than in sunlit leaves. In line with the different role of chlorophyll, sunlit and shaded

559 leaves shows differences in other physiological traits (Figure 8).

560
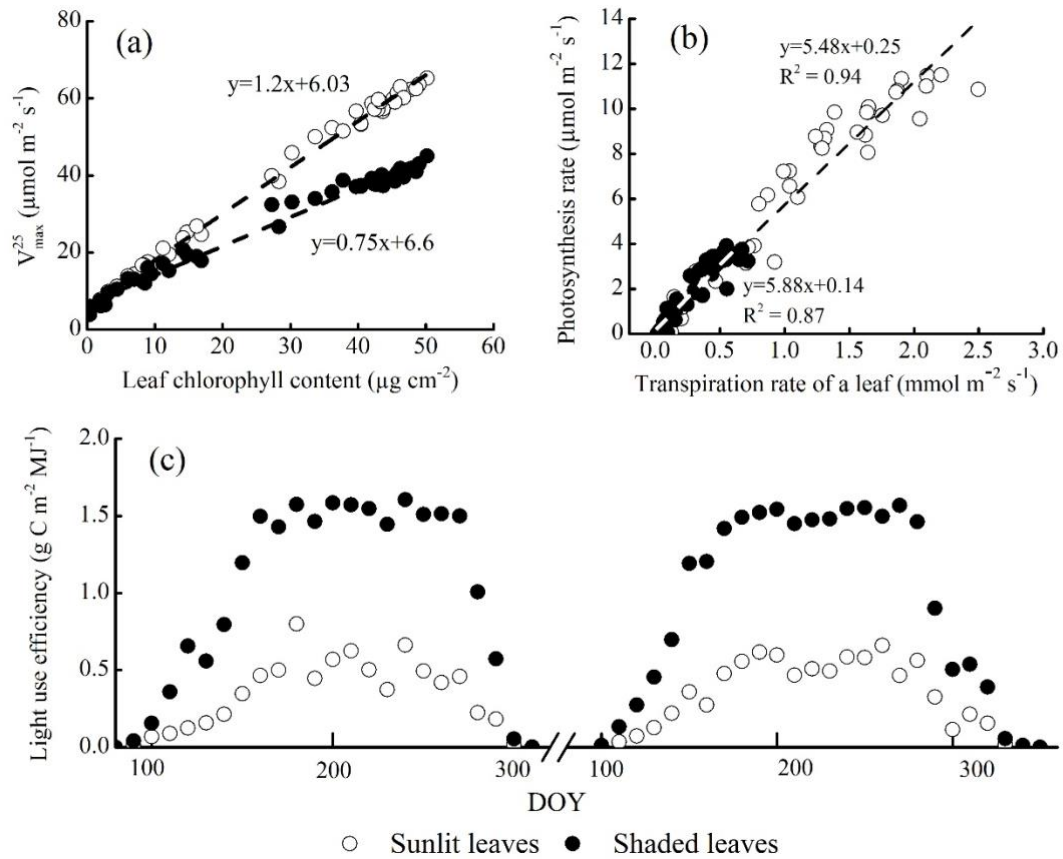
561

Figure 8. Physiological differences, from BEPS simulations, between sunlit and shaded

leaves. (a) V_{max}^{25} versus leaf chlorophyll content; (b) leaf-level photosynthesis versus

transpiration; (c) the seasonal variation in LUE.

566

The seasonal average V_{max}^{25} of a sunlit leaf is 34% higher than that of a shaded leaf, with the

biggest difference of 53% occurring in the middle of the growing seasons (Figure 8a).

According to our modelling results, the carbon and water fluxes of leaves are strongly coupled,

and the water use efficiency (WUE) of the shaded leaf group is similar to that of sunlit leaves

(Figure 8b). For an unit area of leaves, 1 mmol of transpired water could incur 5.5 and 5.8

572 μmols of carbon assimilation for sunlit leaves and shaded leaves, respectively. However, light

573 use efficiency (LUE) of leaves fluctuates with Chl$_{leaf}$ (Croft et al., 2015a; Houborg et al., 2011).

574 According to modelled results from BEPS, the LUE of sunlit leaves ranges from 0.02 to 0.62

575 g C m$_{-2}$ MJ$_{-1}$ APAR with an average of 0.35 g m$_{-2}$ MJ$_{-1}$. Shaded leaves are more efficient in

576 photosynthesis with a LUE ranging from 0.02 to 1.54 g C m$_{-2}$ MJ$_{-1}$, averaging 1.04 g C m$_{-2}$ MJ$_{-}$

577 $_1$ (Figure 8c). These LUE values are within the range of observed and modelled LUE reported

578 previously reported in the literature (Medlyn, 1998; Yuan et al., 2007). Our finding -- that the

579 modelled LUE of shaded leaves is almost 3 times the modelled LUE of sunlit leaves -- echoes

580 the theory that plants are more capable of utilising diffuse radiation than direct radiation (Gu

581 et al., 2002), since shaded leaves only receive diffuse solar radiation for photosynthesis.

582

583 **4. Discussion**

584 **4.1 Improved seasonal representation for GPP and ET simulations**

585 The comparison of the four modelling cases demonstrates that Chl$_{leaf}$ is the best constraint for

586 V_{max}^{25} in the TBM. Seasonal changes in V_{max}^{25} represent changes in the leaf Rubisco content,

587 which is believed to synchronize with the leaf nitrogen pool (Evans, 1989a). In previous studies,

588 leaf structural parameters such as LAI and SLA were used in models to represent seasonal

589 changes in V_{max}^{25}, assuming that LAI and SLA can provide robust representations of the leaf

590 total nitrogen content. However, the seasonal change in leaf total nitrogen varies from the trend

591 of the leaf photosynthetic nitrogen pool (Croft et al., 2017; Migita et al., 2007; Warren et al.,

592 2000), due to disparity between leaf physiological and morphological development shown in

593 Figure 4 (Croft et al., 2014b). As a consequence, it is important to consider leaf photosynthetic

594 nitrogen and its relationship to Rubisco content, rather than merely leaf total nitrogen. In this

595 study, we found that Chl$_{leaf}$ can serve as a direct proxy of the leaf photosynthetic nitrogen pool

596 at the canopy top, thus, can constrain the seasonal variation of V_{max}^{25}. The results also suggest

597 that the accumulation and degradation rates for photosynthetic nitrogen pool (as represented

598 by Chl$_{leaf}$) differ from the rates of changes of leaf and canopy structural components (i.e. LAI

599 and SLA). Consequently, the seasonality of GPP and ET is better explained by Chl$_{leaf}$ than by

600 SLA or LAI, especially during these transitional periods when the disparity between leaf

601 structure and leaf physiology reaches its maximum. In the middle of the growing season, the

602 simulations from four cases are quite similar to each other because leaves were structurally and

603 physiologically mature.

604

605 The seasonality of GPP and ET is also influenced by climatic factors. Though carbon and water

606 fluxes are regulated by the stomata (e.g. Baldocchi 1994; Leuning 1990), our sensitivity

607 analysis finds that GPP and ET are not tightly coupled as expected because of their different

608 sensitivities to non-biological factors. Figure 5 demonstrates that Chl$_{leaf}$ was the dominant

609 factor in controlling the carbon uptake, whereas air temperature and atmospheric mositure

610 demand place the strongest controls on water exchange. This finding was also noted in previous

611 sensitivity studies on several TBMs, which also found V_{max}^{25} is a more influential factor for

612 carbon flux modelling than for water flux modelling (Alton et al., 2007; Ryu et al., 2011). Wang

613 and Dickinson (2012) reviewed observational ET studies across the globe and suggested that

614 available energy and vapor pressure deficit are the two most important factors in determining

615 ET in temperate and boreal forest ecosystems like the Borden site. Consequently, it is

616 reasonable to see that the ET simulations are improved less than the GPP simulations after

617 incorporating Chl$_{leaf}$-based V_{max}^{25} in the TBM.

618

619 **4.2 Physiological differences between sunlit and shaded leaves**

620 Many studies have compared the physiological traits of sun and shade-adapted leaves (e.g.

621 Anderson et al., 1988; Boardman, 1977; Chow and Anderson, 1987) and reported that the

622 constituents of photosynthetic components vary with leaf light environments. Under a saturated

623 light environment, leaves tend to assign more nitrogen to produce Rubisco needed in dark

624 reactions of photosynthesis, while shaded leaves will invest more nutrients in the production

625 of the light-harvesting apparatus to capture the photons needed in light reactions. In a canopy,

626 nitrogen is distributed proportionally from top leaves to bottom leaves following the long-term

627 radiation gradient. The sunlit part of the crown tends to have higher N$_{area}$ to produce more

628 photosynthetic components (e.g. Rubisco) in comparison to the shaded part of the canopy. As

629 such, the leaf physiological traits acclimate to leaf light environments to maximize the overall

630 productivity of the whole canopy. Understanding the influence of the light environment on

631 leaves is an important premise before upscaling modelled GPP and ET from leaf to canopy in

632 structurally complex forests.

633

634 Estimations from BEPS captures the physiological difference between sunlit and shaded leaves

635 (Figure 7 and 8). With an increase in Chl$_{leaf}$, V_{max}^{25} and photosynthesis of shaded leaves

636 increase more slowly than those of sunlit leaves, because shaded leaves are predominantly

637 located at the bottom of the canopy where the relatively low nitrogen content constrains the

638 content of Rubisco. Therefore, the linear relationship between Chl_{leaf} and V_{max}^{25} has a smaller

639 slope for shaded leaves than for sunlit leaves. This finding echoes previous experiments

640 reporting changes in Chl_{leaf} -V_{max}^{25} relationships under different light environments (Table 1).

641

642 **Table 1.** Slopes in the linear Chl_{leaf}–V_{max}^{25} relationships reported in the literatures. Ratios of

643 V_{max}^{25} / Chl_{leaf} in some studies are regarded as slopes. Molecular mass of Chl_{leaf} is 893.5 g

644 mol_{-1}.

Species	Solar irradiance on leaves ($\mu mol\ m_{-2}\ s_{-1}$)	Slopes in Chl_{leaf} –V_{max}^{25} relationships ($\mu mol\ m_{-2}\ s_{-1}$ V_{max}^{25} per $\mu g\ cm_{-2}$ Chl_{leaf})	Reference
Cucumis	1000	1.82	(Evans, 1989b) [a]
	550	1.43	
	260	1.43	
	150	1.01	
Phaseolus	820	2.27	
	220	1.58	
	120	1.32	
Maize		1.12	(Houborg et al., 2015b)
Soybean		1.75	
Sorghum		1.25	
Wheat		2.65	
Common bean		1.99	
Cotton		1.76	
Rice		1.60	
Barley		3.07	
Tobacco		2.82	
Deciduous broad leaf tree species	1265 [b]	1.3	This study
Sunlit leaves	972 [c]	1.2	
Shaded leaves	162 [c]	0.77	

645 [a] J_{max}^{25} is converted into V_{max}^{25} by simply dividing 2;

649

650 The experimental studies included in Table 1 demonstrate that leaf light environments affect

651 the slopes of $Chl_{leaf} - V_{max}^{25}$ relationships to a degree that is almost comparable to the influence

652 brought by species types. While an increase of 1 μg cm$_{-2}$ in Chl_{leaf} may result in 1 to 3 μmol m$_{-}$

653 $_2$ s$_{-1}$ of increases in V_{max}^{25} for different species, a change in the light environment for a given

654 species could dampen its $Chl_{leaf} - V_{max}^{25}$ slope by a factor between 21% and 44%. Meanwhile,

655 our modelled results show that shaded leaves have a 34% lower $Chl_{leaf} - V_{max}^{25}$ slope than sunlit

656 leaves for deciduous broadleaf trees, which is similar to the results from previous limited

657 experimental studies (Evans, 1989b). Therefore, we suggest that our two-leaf TBM is capable

658 of describing the variations in light environments and is reliable for incorporating Chl_{leaf} in

659 structurally complex forests.

660

4. Conclusions

662 Chlorophyll molecules embedded in the light harvesting apparatus are responsible for

663 absorbing solar energy for photosynthesis, and they are also related, through sharing of the leaf

664 nitrogen pool, to the enzyme Rubisco and the cytochrome b6f complex (Cty f) needed by

665 photosynthesis. Based on the key role of chlorophyll in photosynthesis, Chl_{leaf} is regarded as a

666 valuable proxy of the photosynthetic parameters – V_{max}^{25} and J_{max}^{25} – used in TBMs. However,

667 since sun and shade adapted leaves have different strategies in the nitrogen allocation to

668 components of the photosynthetic apparatuses (i.e. chlorophyll and Rubisco), understanding

669 the influence of the light environment on leaves is an important premise before upscaling

670 modelled GPP and ET from leaf to canopy in the structurally complex forests. In this study, we

671 incorporated a time series of measured Chl$_{leaf}$ into a two-leaf TBM named BEPS. The following

672 conclusions are drawn:

673 1. Chl$_{leaf}$ provides a reliable constraint on the seasonal variations of V_{max}^{25} and J_{max}^{25} at a

674 forest site. By incorporating Chl$_{leaf}$–based V_{max}^{25} into BEPS, the biases of simulated annual

675 GPP and annual ET are considerably reduced and the temporal correlations between simulated

676 and measured fluxes are considerably improved relative to three cases using constant V_{max}^{25},

677 LAI-based V_{max}^{25} and SLA-based V_{max}^{25}. The largest improvements in GPP estimates are

678 witnessed in spring and fall, when MAEs are reduced from between 2.2-3.2 to 1.8 g C m$_{-2}$ d$_{-1}$

679 and from between 2.1-2.8 to 1.8 g C m$_{-2}$ d$_{-1}$, respectively. MAEs of modelled ET also shrink

680 from 0.7-0.8 to 0.6 mm d$_{-1}$ in spring while simulated ET does not improve very much in autumn.

681 2. The two-leaf TBM with V_{max}^{25} constrained by Chl$_{leaf}$ is capable of capturing the

682 physiological differences between sunlit leaves and shaded leaves in a forest stand. According

683 to modelled results, a 1 μg cm$_{-2}$ increase in Chl$_{leaf}$ corresponds to a 1.2 μmols m$_{-2}$ s$_{-1}$ increase

684 in V_{max}^{25} in sunlit leaves and a 0.77 μmols m$_{-2}$ s$_{-1}$ increase in V_{max}^{25} in shaded leaves. The result

685 is in line with the plant physiological studies that found plants optimize the nitrogen allocations

686 to different photosynthetic components according to the light environment to maximize the

687 canopy-scale CO$_2$ assimilation rate.

688 This study demonstrates, for the first time, the importance of using chlorophyll in TBMs

689 to reduce the uncertainties in carbon and water flux estimates for forested ecosystems. It also

690 incorporates Chl$_{leaf}$ within a two-leaf scheme to account for the complex light environments

691 inside forest canopies and quantifies the physiological difference between sunlit and shaded

692   leaves.

693

699

700   **Appendix A. Net radiation on sunlit and shaded leaves**

701   In every hourly time step of BEPS, the whole canopy was divided into four groups of leaves

702   based on the location and radiation features of the leaves, namely sunlit leaves in the overstorey,

703   shaded leaves in the overstorey, sunlit leaves in the understorey and shaded leaves in the

704   understorey (Chen et al., 1999; Liu et al., 2003). The leaves in each group have identical

705   features so BEPS could use one leaf to represent one group. Net radiation on a leaf is composed

706   by three sources:

707    $R_{n\_i} = R_{dir\_i} + R_{dif\_i} + R_{l\_i}$ (A1)

708   where R_n is the total net radiation on a certain leaf, R_{dir}, R_{dif} and R_l refers to the net

709   direct incoming solar radiation, net diffuse solar radiation and net longwave radiation on this

710   leaf. i refers to one of the four types of leaves. For a shaded leaf, $R_{dir} = 0$.

711   In order to differentiate the incoming solar radiation into a direct and diffuse part, a semi-

712   empirical equation is applied:

713    $\frac{S_{dif}}{S_g} = \begin{cases} 0.943 + 0.734r - 4.9r^2 + 1.796r^3 + 2.058r^4 & r < 0.8 \\ 0.13 & r \geq 0.8 \end{cases}$ (A2)

36

714     $S_{dir} = S_g - S_{dif}$ (A3)

715   where S_g, S_{dir} and S_{dif} are global solar radiation, incoming direct solar radiation and

716   diffuse solar radiation. r is a parameter used to quantify the cloudiness in sky

717     $r = \dfrac{S_g}{S_0 cos\theta}$ (A4)

718   S_0 is the solar constant set as 1362 W/m2, θ is the solar zenith angel in this hourly time step.

719   The net direct shortwave radiation on the sunlit representative leaf in the overstorey or

720   understorey of the canopy is:

721     $R_{dir\_o\_sunlit} = R_{dir\_u\_sunlit} = (1 - \alpha_L)S_{dir}cos\alpha/cos\theta$ (A5)

722   where α_L is the albedo of leaves. α is the mean leaf-sun angle which is fixed at 60° when

723   the canopy has a spherical leaf distribution.

724   On the other hand, the net diffuse shortwave radiation on the four groups of the leaves are

725   approximated respectively as:

726     $R_{dif\_o\_sunlit} = R_{dif\_o\_shaded} = (1 - \alpha_L)\left(S_{dif}\left[1 - e^{-0.5\Omega LAI_o/cos\bar{\theta}_o}\right]/LAI_o + C_o\right)$ (A6)

727     $R_{dif\_u\_sunlit} = R_{dif\_u\_shaded} = (1 - \alpha_L)(S_{dif}e^{-0.5\Omega LAI_o/cos\bar{\theta}_o}\left[1 - e^{-0.5\Omega LAI_u/cos\bar{\theta}_u}\right]/LAI_u +$

728     $C_u)$ (A7)

729   LAI_o and LAI_u denote the LAI value of the overstorey and the understorey, C_o and C_u are

730   used to quantify the multiple scattering of the direct solar radiation from the leaf (Chen et al.,

731   1999)

732     $C_o = 0.07\Omega S_{dir}(1.1 - 0.1LAI)e^{-cos\theta}$ (A8)

733     $C_u = 0.07\Omega S_{dir}e^{-0.5\Omega LAI_o/cos\theta}(1.1 - 0.1LAI_u)e^{-cos\theta}$ (A9)

734     $\bar{\theta}_o$ and $\bar{\theta}_o$ are the representative zenith angles for diffuse radiation transmission of the

735   overstorey and understorey leaves and slightly dependent on the corresponding LAI (Liu et al.,

736 2003):

$$cos\bar{\theta} = 0.537 + 0.025LAI \tag{A10}$$

738 The net longwave radiation on these leaves is calculated as:

$$R_{L\_o\_sunlit} = R_{L\_o\_shaded} = \frac{1}{LAI_o}\left\{\left\{\varepsilon_o\left[\varepsilon_a\sigma T_a^4 + \varepsilon_u\sigma T_u^4\left(1 - e^{-0.5LAI_u\Omega/cos\bar{\theta}_u}\right) + \right.\right.\right.$$

$$\left.\varepsilon_g\sigma T_g^4 e^{-0.5LAI_u\Omega/cos\bar{\theta}_u}\right] - 2\varepsilon_o\sigma T_o^4\right\}\left(1 - e^{-0.5LAI_o\Omega/cos\bar{\theta}_o}\right) + \varepsilon_o(1 - \varepsilon_u)\left(1 - \right.$$

$$\left.\left. e^{-0.5LAI_u\Omega/cos\bar{\theta}_u}\right)\left[\varepsilon_a\sigma T_a^4 e^{-0.5LAI_o\Omega/cos\bar{\theta}_o} + \varepsilon_o\sigma T_o^4\left(1 - e^{-0.5LAI_o\Omega/cos\bar{\theta}_o}\right)\right]\right\} \tag{A11}$$

742

$$R_{L\_u\_sunlit} = R_{L\_u\_shaded} = \frac{1}{LAI_u}\left\{\left\{\varepsilon_u\left[\varepsilon_a\sigma T_a^4 e^{-0.5LAI_o\Omega/cos\bar{\theta}_o} + \varepsilon_o\sigma T_o^4\left(1 - \right.\right.\right.\right.$$

$$\left. e^{-0.5LAI_o\Omega/cos\bar{\theta}_o}\right) + \varepsilon_g\sigma T_g^4\right] - 2\varepsilon_u\sigma T_u^4\right\}\left(1 - e^{-0.5LAI_u\Omega/cos\bar{\theta}_u}\right) + \varepsilon_u\left(1 - \right.$$

$$\left.\varepsilon_g\right)\left\{\left[\varepsilon_a\sigma T_a^4 e^{-0.5LAI_o\Omega/cos\bar{\theta}_o} + \varepsilon_o\sigma T_o^4\left(1 - e^{-0.5LAI_o\Omega/cos\bar{\theta}_o}\right)\right]e^{-0.5LAI_u\Omega/cos\bar{\theta}_u} + \right.$$

$$\left.\varepsilon_u\sigma T_u^4\left(1 - e^{-0.5LAI_u\Omega/cos\bar{\theta}_u}\right)\right\} + \varepsilon_u(1 - \varepsilon_o)\left[\varepsilon_u\sigma T_u^4\left(1 - e^{-0.5LAI_u\Omega/cos\bar{\theta}_u}\right) + \right.$$

$$\left.\left.\varepsilon_g\sigma T_g^4 e^{-0.5LAI_u\Omega/cos\bar{\theta}_u}\right]\left(1 - e^{-0.5LAI_o\Omega/cos\bar{\theta}_o}\right)\right\} \tag{A12}$$

748 where σ is the Stephen-Boltzmann constant equals to $5.67 \times 10^{-8}Wm^{-2}K^{-4}$. ε_a, ε_o, ε_u

749 and ε_g are the emissivity of the atmosphere, overstory, understory and ground surface,

750 respectively. ε_o, ε_u and ε_g are prescribed as 0.98, 0.98 and 0.95 according to (Chen and

751 Zhang, 1989; Chen et al., 1989), and ε_a is computed as $\varepsilon_a = 1.24(\frac{e_a}{T_a})^{1/7}$(Brutsaert, 1982),

752 where e_a and T_a are water vapor pressure in *mbar* and temperature of the atmosphere in *K*.

753 T_o, T_u and T_g are the temperatures of the overstory, the understorey and ground in *K*.

754

755 **Appendix B. Quantification of the soil water stress factor**

756 To assess the effect of soil water deficit on stomatal conductance (*fw*), a scaling factor based

757 on the ratio of the real time available water in soil to the maximum plant available water (Chen

758 et al., 2005; Wang and Leuning, 1998; Wigmosta et al., 1994) is used to implement the soil

759 water information.

760 $$fw = \begin{cases} 0 & \theta_{sw}(z) < \theta_{wp} \\ \dfrac{\theta_{sw}(z) - \theta_{wp}}{\theta_{fc} - \theta_{wp}} & \theta_{wp} \leq \theta_{sw}(z) \leq \theta_{fc} \\ 1 & \theta_{sw}(z) > \theta_{fc} \end{cases} \qquad (B1)$$

761 where $\theta_{sw}(z)$ is the soil water content of layer z, z often refers to the top 30 cm based on the

762 availability of the soil water measurements. θ_{wp} and θ_{fc} are the wilting point and the field

763 capacity (m3/m3) of the soil layer. θ_{wp} and θ_{fc} are derived by the soil texture information

764 provided on the Fluxnet archive (http://fluxnet.ornl.gov/), the patterns of multi-year soil

765 moisture measurements and the algorithm developed by Saxton and Rawls (2006).

766

767 **Reference**

768 Alton, P., Mercado, L., North, P., 2007. A sensitivity analysis of the land-surface scheme
769   JULES conducted for three forest biomes: Biophysical parameters, model processes, and
770   meteorological driving data, Global Biogeochemical Cycles, 20, GB1008,
771   doi:10.1029/2005GB002653.

772 Alton, P., 2017. Retrieval of seasonal Rubisco-limited photosynthetic capacity at global
773   FLUXNET sites from hyperspectral satellite remote sensing: Impact on carbon modelling,
774   Agricultural and Forest Meteorology, 232, 74-88,
775   http://doi.org/10.1016/j.agrformet.2016.08.001.

776 Amthor, J.S., Chen, J.M., Clein, J.S., Frolking, S.E., Goulden, M.L., Grant, R.F., Kimball, J.S.,
777   King, A.W., McGuire, A.D., Nikolov, N.T., Potter, C.S., Wang, S., Wofsy, S.C., 2001.
778   Boreal forest CO 2 exchange and evapotranspiration predicted by nine ecosystem process
779   models: Intermodel comparisons and relationships to field measurements. Journal of
780   Geophysical Research 106, 33623. doi:10.1029/2000JD900850

781 Anderson, J., Chow, W., Goodchild, D., 1988. Thylakoid Membrane Organisation in Sun/Shade
782   Acclimation. Australian Journal of Plant Physiology 15, 11. doi:10.1071/PP9880011

783 Baldocchi, D., 1994. An analytical solution for coupled leaf photosynthesis and stomatal
784   conductance models, Tree Physiology, 14, 1069–1079, doi:10.1093/treephys/14.7-8-
785   9.1069.

786 Barr, A.G., Black, T.A., Hogg, E.H., Kljun, N., Morgenstern, K., Nesic, Z., 2004. Inter-annual
787   variability in the leaf area index of a boreal aspen-hazelnut forest in relation to net
788   ecosystem production. Agricultural and Forest Meteorology 126, 237–255.
789   doi:10.1016/j.agrformet.2004.06.011

790 Barr, A.G., Richardson, A.D., Hollinger, D.Y., Papale, D., Arain, M.A., Black, T.A., et al., 2013.
791   Use of change-point detection for friction–velocity threshold evaluation in eddy-
792   covariance studies. Agric. For. Meteorol. 171–172, 31–45.

793 Boardman, N.K., 1977. Comparative Photosynthesis of Sun and Shade Plants. Annual Review
794   of Plant Physiology 28, 355–377. doi:10.1146/annurev.pp.28.060177.002035

795 Brutsaert, W., 1982. Evaporation into the Atmosphere. Springer Netherlands, Dordrecht.
796   doi:10.1007/978-94-017-1497-6

797 Chen, B., Chen, J.M., Ju, W., 2007. Remote sensing-based ecosystem-atmosphere simulation
798   scheme (EASS)-Model formulation and test with multiple-year data. Ecological
799   Modelling 209, 277–300. doi:10.1016/j.ecolmodel.2007.06.032

800 Chen, B., Liu, J., Chen, J.M., Croft, H., Gonsamo, A., He, L., Luo, X., 2016. Assessment of
801   foliage clumping effects on evapotranspiration estimates in forested ecosystems,
802   Agricultural and Forest Meteorology, 216, 82-92.

803 Chen, J.M., Zhang, R.H., 1989. Studies on the measurements of crop emissivity and sky
804   temperature. Agricultural and Forest Meteorology 49, 23–34. doi:10.1016/0168-
805   1923(89)90059-2

806 Chen, J.., Liu, J., Cihlar, J., Goulden, M.., 1999. Daily canopy photosynthesis model through
807   temporal and spatial scaling for remote sensing applications. Ecological Modelling 124,
808   99–119. doi:10.1016/S0304-3800(99)00156-8

809 Chen, J.M., Chen, X., Ju, W., Geng, X., 2005. Distributed hydrological model for mapping
810   evapotranspiration using remote sensing inputs. Journal of Hydrology 305, 15–39.
811   doi:10.1016/j.jhydrol.2004.08.029

812 Chen, J.M., Cihlar, J., 1995. Plant canopy gap-size analysis theory for improving optical
813   measurements of leaf-area index. Applied optics 34, 6211–6222.
814   doi:10.1364/AO.34.006211

815 Chen, J.M., Mo, G., Pisek, J., Liu, J., Deng, F., Ishizawa, M., Chan, D., 2012. Effects of foliage
816   clumping on the estimation of global terrestrial gross primary productivity. Global
817   Biogeochemical Cycles 26, 1–18. doi:10.1029/2010GB003996

818 Chen, J.M., Yang, B.J., Zhang, R.H., 1989. Soil thermal emissivity as affected by its water
819   content and surface treatment. Soil science (USA).

820 Chow, W.S., Anderson, J.M., 1987. Photosynthetic responses of Pisum sativum to an increase
821   in irradiance during growth. II. Thylakoid membrane components. Functional Plant
822   Biology 14, 9–19. doi:doi:10.1071/PP9870009

823 Croft, H., Chen, J.M., Froelich, N.J., Chen, B., Staebler, R.M., 2015a. Seasonal controls of
824   canopy chlorophyll content on forest carbon uptake: Implications for GPP modeling.
825   Journal of Geophysical Research: Biogeosciences 120, n/a-n/a.
826   doi:10.1002/2015JG002980

827 Croft, H., Chen, J.M., Luo, X., Barlett, P., Chen, B., Staebler, R.M., n.d. Leaf chlorophyll

828   content as a proxy for leaf photosynthetic capacity. Global Change Biology.

829 Croft, H., Chen, J.M., Zhang, Y., 2014a. The applicability of empirical vegetation indices for
830   determining leaf chlorophyll content over different leaf and canopy structures. Ecological
831   Complexity 17, 119–130. doi:10.1016/j.ecocom.2013.11.005

832 Croft, H., Chen, J.M., Zhang, Y., 2014b. Temporal disparity in leaf chlorophyll content and leaf
833   area index across a growing season in a temperate deciduous forest. International Journal
834   of Applied Earth Observation and Geoinformation 33, 312–320.
835   doi:10.1016/j.jag.2014.06.005

836 Croft, H., Chen, J.M., Zhang, Y., Simic, A., 2013. Modelling leaf chlorophyll content in
837   broadleaf and needle leaf canopies from ground, CASI, Landsat TM 5 and MERIS
838   reflectance data. Remote Sensing of Environment 133, 128–140.
839   doi:10.1016/j.rse.2013.02.006

840 Croft, H., Chen, J.M., Zhang, Y., Simic, A., Noland, T.L., Nesbitt, N., Arabian, J., 2015b.
841   Evaluating leaf chlorophyll content prediction from multispectral remote sensing data
842   within a physically-based modelling framework. ISPRS Journal of Photogrammetry and
843   Remote Sensing 102, 85–95. doi:10.1016/j.isprsjprs.2015.01.008

844 De Pury, D.G.G., Farquhar, G.D., 1997. Simple scaling of photosynthesis from leaves to
845   canopies without the errors of big-leaf models. Plant, Cell and Environment 20, 537–557.
846   doi:10.1111/j.1365-3040.1997.00094.x

847 Demarez, V., Gastellu-Etchegorry, J.P., Mogin, E., Marty, G., Proisy, C., Dufréne, E., Dantec,
848   V. Le, 1999. Seasonal variation of leaf chlorophyll content of a temperate forest. Inversion
849   of the PROSPECT model. International Journal of Remote Sensing 20, 879–894.

850 Ethier, G.J., Livingston, N.J., 2004. On the need to incorporate sensitivity to CO_2 transfer
851   conductance into the Farquhar-von Caemmerer-Berry leaf photosynthesis model. Plant,
852   Cell and Environment 27, 137–153. doi:10.1111/j.1365-3040.2004.01140.x

853 Evans, J., 1989a. Photosynthesis and nitrogen relationships in leaves of C3 plants. Oecologia
854   78, 9–19. doi:10.1007/BF00377192

855 Evans, J., 1989b. Partitioning of Nitrogen Between and Within Leaves Grown Under Different
856   Irradiances. Australian Journal of Plant Physiology 16, 533. doi:10.1071/PP9890533

857 Farquhar, G.D., von Caemmerer, S., Berry, J.A., 1980. A biochemical model of photosynthetic
858   CO_2 assimilation in leaves of C 3 species. Planta 149, 78–90. doi:10.1007/BF00386231

859 Field, C., 1983. Allocating leaf nitrogen for the maximization of carbon gain: Leaf age as a
860   control on the allocation program. Oecologia 56, 341–347. doi:10.1007/BF00379710

861 Froelich, N., Croft, H., Chen, J.M., Gonsamo, A., Staebler, R.M., 2015. Trends of carbon fluxes
862   and climate over a mixed temperate–boreal transition forest in southern Ontario, Canada.
863   Agricultural and Forest Meteorology 211–212, 72–84.
864   doi:10.1016/j.agrformet.2015.05.009

865 Gitelson, A.A., Viña, A., Ciganda, V., Rundquist, D.C., Arkebauer, T.J., 2005. Remote

866   estimation of canopy chlorophyll content in crops. Geophysical Research Letters 32,
867   L08403. doi:10.1029/2005GL022688

868 Gitelson, A.A., Viña, A., Verma, S.B., Rundquist, D.C., Arkebauer, T.J., Keydan, G., Leavitt,
869   B., Ciganda, V., Burba, G.G., Suyker, A.E., 2006. Relationship between gross primary
870   production and chlorophyll content in crops: Implications for the synoptic monitoring of
871   vegetation productivity. Journal of Geophysical Research Atmospheres 111, 1–13.
872   doi:10.1029/2005JD006017

873 Gonsamo, A., Chen, J.M., Price, D.T., Kurz, W. a., Liu, J., Boisvenue, C., Hember, R. a., Wu,
874   C., Chang, K.H., 2013. Improved assessment of gross and net primary productivity of
875   Canada's landmass. Journal of Geophysical Research: Biogeosciences 118, 1546–1560.
876   doi:10.1002/2013JG002388

877 Gonsamo, A., Croft, H., Chen, J.M., Wu, C., Froelich, N., Staebler, R.M., 2015. Radiation
878   contributed more than temperature to increased decadal autumn and annual carbon uptake
879   of two eastern North America mature forests. Agricultural and Forest Meteorology 201,
880   8–16. doi:10.1016/j.agrformet.2014.11.007

881 Grant, R.F., Zhang, Y., Yuan, F., Wang, S., Hanson, P.J., Gaumont-Guay, D., Chen, J., Black, T.
882   a., Barr, a., Baldocchi, D.D., Arain, a., 2006. Intercomparison of techniques to model
883   water stress effects on CO2 and energy exchange in temperate and boreal deciduous
884   forests. Ecological Modelling 196, 289–312. doi:10.1016/j.ecolmodel.2006.02.035

885 Groenendijk, M., Dolman, A.J., Ammann, C., Arneth, A., Cescatti, A., Dragoni, D., Gash,
886   J.H.C., Gianelle, D., Gioli, B., Kiely, G., Knohl, A., Law, B.E., Lund, M., Marcolla, B.,
887   van der Molen, M.K., Montagnani, L., Moors, E., Richardson, A.D., Roupsard, O.,
888   Verbeeck, H., Wohlfahrt, G., 2011. Seasonal variation of photosynthetic model parameters
889   and leaf area index from global Fluxnet eddy covariance data. Journal of Geophysical
890   Research 116, G04027. doi:10.1029/2011JG001742

891 Gu, L., Baldocchi, D., Verma, S.B., Black, T.A., Vesala, T., Falge, E.M., Dowty, P.R., 2002.
892   Advantages of diffuse radiation for terrestrial ecosystem productivity. Journal of
893   Geophysical Research: Atmospheres 107, ACL 2-1. doi:10.1029/2001JD001242

894 Hikosaka, K., 2014. Optimal nitrogen distribution within a leaf canopy under direct and diffuse
895   light. Plant, cell & environment 37, 2077–85. doi:10.1111/pce.12291

896 Hikosaka, K., Terashima, I., 1996. Nitrogen partitioning among photosynthetic components
897   and its consequenses in sun and shade plants. Functional Ecology 10, 335–343.
898   doi:10.2307/2390281

899 Hikosaka, K., Terashima, I., 1995. A model of the acclimation of photosynthesis in the leaves
900   of C3 plants to sun and shade with respect to nitrogen use. Plant, Cell and Environment
901   18, 605–618. doi:10.1111/j.1365-3040.1995.tb00562.x

902 Hirose, T., Werger, M.J. a, 1987. Maximizing dialy canopy phoytosynthesis with respect to the
903   leaf nitrogen allocation pattern in the canopy. Oecologia 72, 520–526.
904   doi:10.1007/BF00378977

905 Houborg, R., Anderson, M.C., Daughtry, C.S.T., Kustas, W.P., Rodell, M., 2011. Using leaf
906   chlorophyll to parameterize light-use-efficiency within a thermal-based carbon, water and
907   energy exchange model. Remote Sensing of Environment 115, 1694–1705.
908   doi:10.1016/j.rse.2011.02.027

909 Houborg, R., Cescatti, A., Migliavacca, M., Kustas, W.P., 2013. Satellite retrievals of leaf
910   chlorophyll and photosynthetic capacity for improved modeling of GPP. Agricultural and
911   Forest Meteorology 177, 10–23. doi:10.1016/j.agrformet.2013.04.006

912 Houborg, R., McCabe, M., Cescatti, A., Gao, F., Schull, M., Gitelson, A., 2015a. Joint leaf
913   chlorophyll content and leaf area index retrieval from Landsat data using a regularized
914   model inversion system (REGFLEC). Remote Sensing of Environment 159, 203–221.
915   doi:10.1016/j.rse.2014.12.008

916 Houborg, R., McCabe, M.F., Cescatti, A., Gitelson, A.A., 2015b. Leaf chlorophyll constraint
917   on model simulated gross primary productivity in agricultural systems. International
918   Journal of Applied Earth Observation and Geoinformation 43, 160–176.
919   doi:10.1016/j.jag.2015.03.016

920 Iio, A., Fukasawa, H., Nose, Y., Kato, S., Kakubari, Y., 2005. Vertical, horizontal and azimuthal
921   variations in leaf photosynthetic characteristics within a Fagus crenata crown in relation
922   to light acclimation. Tree physiology 25, 533–544. doi:10.1093/treephys/25.5.533

923 Ju, W., Chen, J.M., Black, T.A., Barr, A.G., Liu, J., Chen, B., 2006. Modelling multi-year
924   coupled carbon and water fluxes in a boreal aspen forest. Agricultural and Forest
925   Meteorology 140, 136–151. doi:10.1016/j.agrformet.2006.08.008

926 Jung, M., Reichstein, M., Ciais, P., Seneviratne, S.I., Sheffield, J., Goulden, M.L., Bonan, G.,
927   Cescatti, A., Chen, J., de Jeu, R., Dolman, a J., Eugster, W., Gerten, D., Gianelle, D.,
928   Gobron, N., Heinke, J., Kimball, J., Law, B.E., Montagnani, L., Mu, Q., Mueller, B.,
929   Oleson, K., Papale, D., Richardson, A.D., Roupsard, O., Running, S., Tomelleri, E., Viovy,
930   N., Weber, U., Williams, C., Wood, E., Zaehle, S., Zhang, K., 2010. Recent decline in the
931   global land evapotranspiration trend due to limited moisture supply. Nature 467, 951–954.
932   doi:10.1038/nature09396

933 Kalacska, M., Lalonde, M., Moore, T.R., 2015. Estimation of foliar chlorophyll and nitrogen
934   content in an ombrotrophic bog from hyperspectral data: Scaling from leaf to image.
935   Remote Sensing of Environment 169, 270–279. doi:10.1016/j.rse.2015.08.012

936 Kattge, J., Knorr, W., Raddatz, T., Wirth, C., 2009. Quantifying photosynthetic capacity and its
937   relationship to leaf nitrogen content for global-scale terrestrial biosphere models. Global
938   Change Biology 15, 976–991. doi:10.1111/j.1365-2486.2008.01744.x

939 Knyazikhin, Y., Schull, M.A., Stenberg, P., Mõttus, M., Rautiainen, M., Yang, Y., Marshak, A.,
940   Latorre Carmona, P., Kaufmann, R.K., Lewis, P., Disney, M.I., Vanderbilt, V., Davis, A.B.,
941   Baret, F., Jacquemoud, S., Lyapustin, A., Myneni, R.B., 2013. Hyperspectral remote
942   sensing of foliar nitrogen content. Proceedings of the National Academy of Sciences of
943   the United States of America 110, E185-92. doi:10.1073/pnas.1210196109

944 Koffi, E.N., Rayner, P.J., Norton, A.J., Frankenberg, C., and Scholze, M., 2015. Investigating

945 the usefulness of satellite-derived fluorescence data in inferring gross primary
946 productivity within the carbon cycle data assimilation system, Biogeosciences, 12, 4067-
947 4084, doi:10.5194/bg-12-4067-2015

948 Kull, O., 2002. Acclimation of photosynthesis in canopies: models and limitations. Oecologia
949 133, 267–279. doi:10.1007/s00442-002-1042-1

950 Lambers, H., Chapin, F.S., Pons, T.L., 2008. Plant Physiological Ecology. Springer New York,
951 New York, NY. doi:10.1007/978-0-387-78341-3

952 Lee, X., Fuentes, J.D., Staebler, R.M., Neumann, H.H., 1999. Long-term observation of the
953 atmospheric exchange of CO 2 with a temperate deciduous forest in southern Ontario,
954 Canada. Journal of Geophysical Research 104, 15975. doi:10.1029/1999JD900227

955 Leuning, R., 1990. Modelling Stomatal Behaviour and and Photosynthesis of Eucalyptus
956 grandis, Australian Journal of Plant Physiology, 17, 159–175, doi:10.1071/PP9900159.

957 Lichtenthaler, H.K., Ač, A., Marek, M. V., Kalina, J., Urban, O., 2007. Differences in pigment
958 composition, photosynthetic rates and chlorophyll fluorescence images of sun and shade
959 leaves of four tree species. Plant Physiology and Biochemistry 45, 577–588.
960 doi:10.1016/j.plaphy.2007.04.006

961 Liu, J., Chen, J.M., Cihlar, J., 2003. Mapping evapotranspiration based on remote sensing: An
962 application to Canada's landmass. Water Resources Research 39.
963 doi:10.1029/2002WR001680

964 Luo, X., Chen, J.M., Liu, J., Black, T.A., Croft, H., Staebler, R., He, L., Arain, M.A., Chen, B.,
965 Mo, G., Gonsamo, A., McCaughey, H., 2017. Comparing big-leaf scheme, two-big-leaf
966 scheme and two-leaf scheme for evapotranspiration estimation through coupled carbon-
967 water modelling. Water Resources Research, in review.

968 Medlyn, B.E., 1998. Physiological basis of the light use efficiency model. Tree Physiology 18,
969 167–176. doi:10.1093/treephys/18.3.167

970 Medlyn, B.E., Badeck, F.-W., De Pury, D.G.G., Barton, C.V.M., Broadmeadow, M., Ceulemans,
971 R., De Angelis, P., Forstreuter, M., Jach, M.E., Kellomäki, S., Laitat, E., Marek, M.,
972 Philippot, S., Rey, A., Strassemeyer, J., Laitinen, K., Liozon, R., Portier, B., Roberntz, P.,
973 Wang, K., Jstbid, P.G., 1999. Effects of elevated [CO2] on photosynthesis in European
974 forest species: a meta-analysis of model parameters. Plant, Cell & Environment 22, 1475–
975 1495. doi:10.1046/j.1365-3040.1999.00523.x

976 Niinemets, U., 1997. Acclimation to low irradiance in Picea abies: influences of past and
977 present light climate on foliage structure and function. Tree physiology 17, 723–32.
978 doi:10.1093/treephys/17.11.723

979 Norman, J.M., 1982. Biometeorology in Integrated Pest Management, Biometeorology in
980 Integrated Pest Management. Elsevier. doi:10.1016/B978-0-12-332850-2.50009-8

981 Oki, T., Kanae, S., 2006. Global hydrological cycles and world water resources. Science (New
982 York, N.Y.) 313, 1068–1072. doi:10.1126/science.1128845

983 Pan, Y., Birdsey, R.A., Phillips, O.L., Jackson, R.B., 2013. The Structure, Distribution, and
984   Biomass of the World's Forests. Annual Review of Ecology, Evolution, and Systematics
985   44, 593–622. doi:10.1146/annurev-ecolsys-110512-135914

986 Porcar-Castell, A., Tyystjärvi, E., Atherton, J., Van Der Tol, C., Flexas, J., Pfündel, E.E.,
987   Moreno, J., Frankenberg, C., Berry, J.A., 2014. Linking chlorophyll a fluorescence to
988   photosynthesis for remote sensing applications: Mechanisms and challenges. Journal of
989   Experimental Botany 65, 4065–4095. doi:10.1093/jxb/eru191

990 Potter, C.S., Wang, S., Nikolov, N.T., McGuire, A.D., Liu, J., King, A.W., Kimball, J.S., Grant,
991   R.F., Frolking, S.E., Clein, J.S., Chen, J.M., Amthor, J.S., 2001. Comparison of boreal
992   ecosystem model sensitivity to variability in climate and forest site parameters. Journal of
993   Geophysical Research 106, 33671. doi:10.1029/2000JD000224

994 Ryu, Y., Baldocchi, D.D., Kobayashi, H., van Ingen, C., Li, J., Black, T.A., Beringer, J., van
995   Gorsel, E., Knohl, A., Law, B.E., Roupsard, O., 2011. Integration of MODIS land and
996   atmosphere products with a coupled-process model to estimate gross primary productivity
997   and evapotranspiration from 1 km to global scales. Global Biogeochemical Cycles 25,
998   n/a-n/a. doi:10.1029/2011GB004053

999 Sage, R.F., Pearcy, R.W., Seemann, J.R., 1987. The Nitrogen Use Efficiency of C(3) and C(4)
1000   Plants : III. Leaf Nitrogen Effects on the Activity of Carboxylating Enzymes in
1001   Chenopodium album (L.) and Amaranthus retroflexus (L.). Plant physiology 85, 355–9.

1002 Saxton, K.E., Rawls, W.J., 2006. Soil Water Characteristic Estimates by Texture and Organic
1003   Matter for Hydrologic Solutions. Soil Science Society of America Journal 70, 1569.
1004   doi:10.2136/sssaj2005.0117

1005 Schaefer, K., Schwalm, C.R., Williams, C., Arain, M.A., Barr, A., Chen, J.M., Davis, K.J.,
1006   Dimitrov, D., Hilton, T.W., Hollinger, D.Y., Humphreys, E., Poulter, B., Raczka, B.M.,
1007   Richardson, A.D., Sahoo, A., Thornton, P., Vargas, R., Verbeeck, H., Anderson, R., Baker,
1008   I., Black, T.A., Bolstad, P., Chen, J., Curtis, P.S., Desai, A.R., Dietze, M., Dragoni, D.,
1009   Gough, C., Grant, R.F., Gu, L., Jain, A., Kucharik, C., Law, B., Liu, S., Lokipitiya, E.,
1010   Margolis, H.A., Matamala, R., McCaughey, J.H., Monson, R., Munger, J.W., Oechel, W.,
1011   Peng, C., Price, D.T., Ricciuto, D., Riley, W.J., Roulet, N., Tian, H., Tonitto, C., Torn, M.,
1012   Weng, E., Zhou, X., 2012. A model-data comparison of gross primary productivity:
1013   Results from the North American Carbon Program site synthesis. Journal of Geophysical
1014   Research 117, G03010. doi:10.1029/2012JG001960

1015 Sharkey, T.D., Bernacchi, C.J., Farquhar, G.D., Singsaas, E.L., 2007. Fitting photosynthetic
1016   carbon dioxide response curves for C3 leaves. Plant, Cell and Environment 30, 1035–
1017   1040. doi:10.1111/j.1365-3040.2007.01710.x

1018 Sinclair, T.R., Murphy, C.E., Knoerr, K.R., 1976. Development and Evaluation of Simplified
1019   Models for Simulating Canopy Photosynthesis and Transpiration. Journal of Applied
1020   Ecology 13, 813–829.

1021 Staebler, R.M., Fitzjarrald, D.R., 2004. Observing subcanopy CO2 advection. Agricultural and
1022   Forest Meteorology 122, 139–156. doi:10.1016/j.agrformet.2003.09.011

Teklemariam, T., Staebler, R.M., Barr, A.G., 2009. Eight years of carbon dioxide exchange above a mixed forest at Borden, Ontario. Agricultural and Forest Meteorology 149, 2040–2053. doi:10.1016/j.agrformet.2009.07.011

Terashima, I., Evans, J., 1988. Effects of light and nitrogen nutrition on the organization of the photosynthetic apparatus in spinach. Plant and Cell Physiology 29, 143–155.

Thornton, P.E., Zimmermann, N.E., 2007. An improved canopy integration scheme for a Land Surface Model with prognostic canopy structure. Journal of Climate 20, 3902–3923. doi:10.1175/JCLI4222.1

Walker, A.P., Beckerman, A.P., Gu, L., Kattge, J., Cernusak, L.A., Domingues, T.F., Scales, J.C., Wohlfahrt, G., Wullschleger, S.D., Woodward, F.I., 2014. The relationship of leaf photosynthetic traits - V cmax and J max - to leaf nitrogen, leaf phosphorus, and specific leaf area: a meta-analysis and modeling study. Ecology and evolution 4, 3218–35. doi:10.1002/ece3.1173

Walters, R.G., 2005. Towards an understanding of photosynthetic acclimation. Journal of experimental botany 56, 435–47. doi:10.1093/jxb/eri060

Wang, K., Dickinson, R. E., 2012. A review of global terrestrial evapotranspiration: observation, modelling, climatology, and climatic variability, Review of Geophysics, 50(2011), 1–54

Wang, Y.-P., Leuning, R., 1998. A two-leaf model for canopy conductance, photosynthesis and partitioning of available energy I: Agricultural and Forest Meteorology 91, 89–111. doi:10.1016/S0168-1923(98)00061-6

Warren, C.R., Adams, M.A., 2001. Distribution of N, Rubisco and photosynthesis in Pinus pinaster and acclimation to light. Plant, Cell and Environment 24, 597–609. doi:10.1046/j.1365-3040.2001.00711.x

Webb, E.K., Pearman, G.I., Leuning, R., 1980. Correction of flux measurements for density effects due to heat and water vapour transfer. Quarterly Journal of the Royal Meteorological Society 106, 85–100. doi:10.1002/qj.49710644707

Wellburn, A. R. 1994. The spectral determination of chlorophylls a and b, as well as total carotenoids, using various solvents with spectrophotometers of different resolution, Journal of Plant Physiology, 144, 307–313.

Wigmosta, M.S., Vail, L.W., Lettenmaier, D.P., 1994. A distributed hydrology-vegetation model for complex terrain. Water Resources Research 30, 1665–1679. doi:10.1029/94WR00436

Wilson, K.B., Baldocchi, D.D., Hanson, P.J., 2000. Spatial and seasonal variability of photosynthetic parameters and their relationship to leaf nitrogen in a deciduous forest. Tree Physiology 20, 565–578. doi:10.1093/treephys/20.9.565

Wu, C., Niu, Z., Tang, Q., Huang, W., 2008. Estimating chlorophyll content from hyperspectral vegetation indices: Modeling and validation. Agricultural and Forest Meteorology 148, 1230–1241. doi:10.1016/j.agrformet.2008.03.005

Wullschleger, S.D., 1993. Biochemical Limitations to Carbon Assimilation in C 3 Plants—A Retrospective Analysis of the A/C i Curves from 109 Species. Journal of Experimental Botany 44, 907–920. doi:10.1093/jxb/44.5.907

Xu, L., Baldocchi, D.D., 2003. Seasonal trends in photosynthetic parameters and stomatal conductance of blue oak (Quercus douglasii) under prolonged summer drought and high temperature. Tree Physiology 23, 865–877. doi:10.1093/treephys/23.13.865

Yang, X., Tang, J., Mustard, J.F., Wu, J., Zhao, K., Serbin, S., Lee, J.E., 2016. Seasonal variability of multiple leaf traits captured by leaf spectroscopy at two temperate deciduous forests. Remote Sensing of Environment 179, 1–12. doi:10.1016/j.rse.2016.03.026

Yuan, W., Liu, S., Zhou, G., Zhou, G., Tieszen, L.L., Baldocchi, D., Bernhofer, C., Gholz, H., Goldstein, A.H., Goulden, M.L., Hollinger, D.Y., Hu, Y., Law, B.E., Stoy, P.C., Vesala, T., Wofsy, S.C., 2007. Deriving a light use efficiency model from eddy covariance flux data for predicting daily gross primary production across biomes. Agricultural and Forest Meteorology 143, 189–207. doi:10.1016/j.agrformet.2006.12.001

Zhang, Y., Chen, J.M., Thomas, S.C., 2007. Retrieving seasonal variation in chlorophyll content of overstory and understory sugar maple leaves from leaf-level hyperspectral data. Canadian Journal of Remote Sensing 33, 406–415. doi:10.5589/m07-037